Research at MANA

42 Selected Research Results

2007 - 2017

International Center for
Materials Nanoarchitectonics (MANA)

Research at MANA
42 Selected Research Results

2007-2017

Preface

Ten years have passed since our International Center for Materials Nanoarchitectonics (MANA) was established in October 2007 as one of the initial five research centers in the framework of the World Premier International Research Center Initiative (WPI Program), which is sponsored by Japan's Ministry of Education, Culture, Sports, Science and Technology (MEXT). Commemorating this 10^{th} anniversary of MANA, we have already published a booklet titled "The 10 Year History of MANA" separately.

The present booklet "Research at MANA: 42 Selected Research Results" is its companion piece, in which typical research results obtained at MANA in the past ten years are described briefly. Over this entire 10 year period, MANA has conducted its research based on our own "nanoarchitectonics" concept. Although the research at MANA was carried out in five research fields (Nano-Materials, Nano-System, Nano-Power, Nano-Life, and Nano-Theory), the 42 selected research results in this booklet are classified into three categories: I. Creation of New Fields of Research, II. Fusion of Interdisciplinary Research Fields, and III. Other Remarkable Research Results.

On behalf of all the researchers of MANA, I hope that the research results described in this booklet will be a strong inspiration for your work in the future.

Msakazu Aono

Director-General
WPI Center for Materials Nanoarchitectonics (MANA)
National Institute for Materials Science (NIMS)
Tsukuba, Japan

I Creation of New Fields of Research

Nanosheet-based Nanoarchitectonics for Creating Novel Materials

Atomic Switch and Related Nanoarchitectonic Devices and Systems

Single-molecule-level Memory and Logic Devices

Innovative Nano- and Molecular-scale Characterization/Detection Methods

II Fusion of Interdisciplinary Research Fields

Nano-life Science Inspired by Nanoarchitectonics

Nanoarchitectonics Inspired by Nano-life Science

Fusion of Science and Practical Technology

Theory-Experiment 'Cross-linkage' for Exploring Novel Nanomaterials

III Other Remarkable Research Results

I

Creation of New Fields of Research

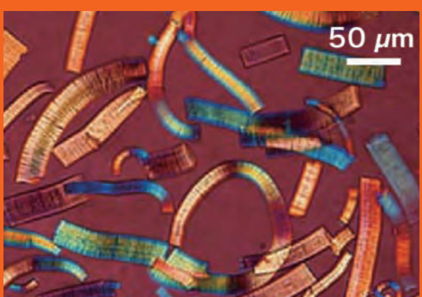

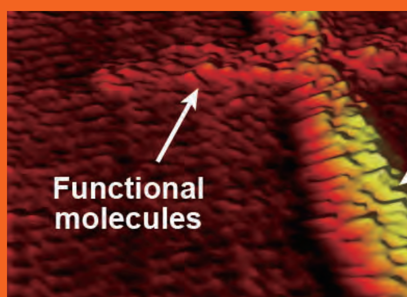

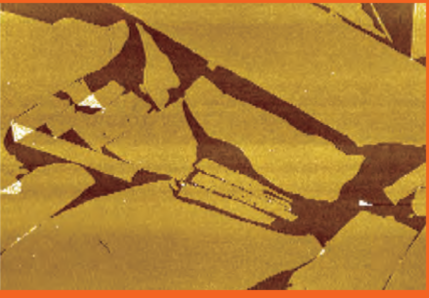

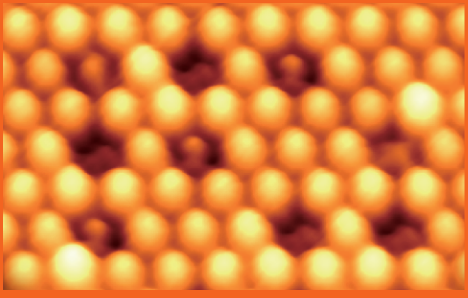

01 Synthesis of 2D nanosheets via massive swelling and exfoliation of layered crystals

T. Sasaki, Y. Ebina, R. Ma

We developed 2D oxide and hydroxide nanosheets by inducing enormous swelling of the starting layered materials. The swollen crystals were disintegrated into molecularly thin elementary layers with very high 2D anisotropy. The colloidal nanosheets were applied in "material nanoarchitectonics" to develop hierarchical materials with unique, advanced functionalities.

Recently, graphene-related 2D materials known as "beyond graphene" have received increasing attention. Oxide and hydroxide nanosheets are promising candidates because they are expected to exhibit many important properties. We found that platy microcrystals of layered metal oxides undergo more than 100-fold accordion-like expansion in aqueous amine solutions, induced via even permeation of the solution into the interlayer gallery to prop it open[1]. Interestingly, the degree of swelling is not dependent on amine agents, while the stability of the swollen crystals is. We controlled their delamination to produce unilamellar oxide nanosheets in high yield[2]. Starting from layered metal oxides synthesized in a specific composition, structure, and size, we obtained high-quality oxide nanosheets, with $Ti_{0.87}O_2$, $Ca_2Nb_3O_{10}$, and $Cs_4W_{11}O_{36}$ as typical examples.

We also developed synthetic routes to produce hydroxide nanosheets based on transition metal or rare earth elements. One achievement was the synthesis of all-transition metal hydroxide nanosheets of $M^{2+}_{(1-x)}M^{3+}_{x}(OH)_2$, where M = Co, Fe, Ni, Mn. We first synthesized brucite-type layered hydroxides based on divalent metal ions via homogeneous precipitation, which were chemically oxidized into the layered double-hydroxide (LDH) structure. The LDH sample was then delaminated into unilamellar nanosheets by treatment with organic solvents such as formamide.

Through those processes, we produced a range of colloidal suspensions of monodisperse 2D nanosheets, which are useful building modules to fabricate functional materials and nanodevices. Fascinating electronic and optical functionalities were revealed with oxide nanosheets. Superior electrochemical and electrocatalytic performance in transition metal-based hydroxide nanosheets after alternate assembly with graphene was seen[3].

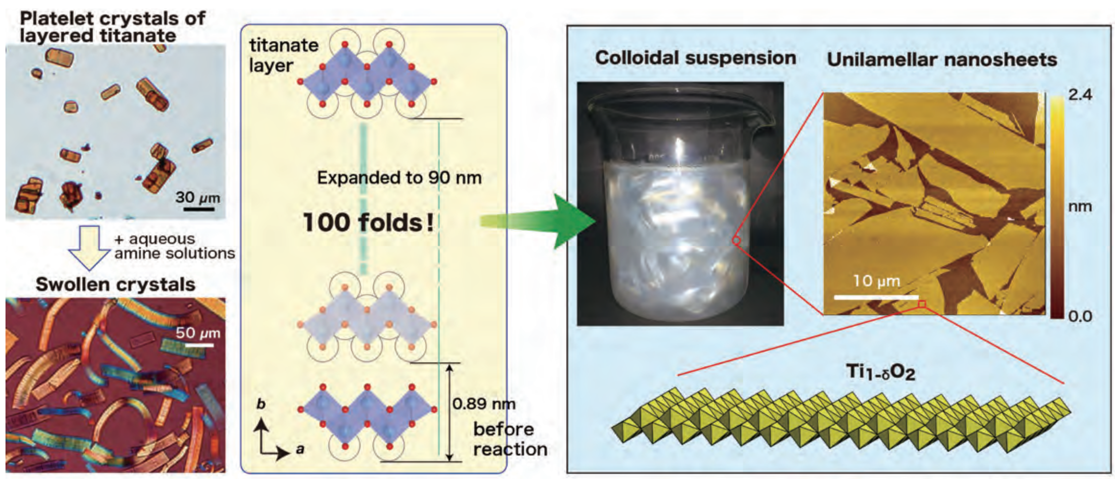

Fig. 1 The swelling to delamination process for the production of oxide nanosheets.

Main Papers

1) "Unusually stable ~100-fold reversible and instantaneous swelling of inorganic layered materials", F. Geng, R. Ma, A. Nakamura, K. Akatsuka, Y. Ebina, Y. Yamauchi, N. Miyamoto, Y. Tateyama, T. Sasaki, *Nat. Commun.* **4** (2013) 1632.
2) "Gigantic swelling of inorganic layered materials: a bridge to molecularly thin two-dimensional nanosheets", F. Geng, R. Ma, Y. Ebina, Y. Yamauchi, N. Miyamoto, T. Sasaki, *J. Am. Chem. Soc.* **136** (2014) 5491.
3) "Molecular-scale heteroassembly of redoxable hydroxide nanosheets and conductive graphene into superlattice composites for high-performance supercapacitors", R. Ma, X. Liu, J. Liang, Y. Bando, T. Sasaki, *Adv. Mater.* **26** (2014) 4173.

02 Nanosheet architectonics: new 2D electronics beyond graphene

M. Osada, T. Sasaki

We developed high-*k* oxide nanosheets, an important material platform for ultrascale electronic devices and post-graphene technology. The new nanosheets (Ti_2NbO_7, $[Ca,Sr]_2Nb_3O_{10}$) provide the highest permittivity (ε_r = 210–320) of all known dielectrics in the ultrathin region (< 10 nm). Layer-by-layer engineering of these nanosheets enabled us to design 2D dielectric devices that cannot be achieved in graphene and other materials. Graphene is only the tip of the iceberg, and we are now starting to discover new possibilities afforded by 2D oxide nanosheets.

2D nanosheets with atomic or molecular thickness are emerging as important new electronic materials owing to their fascinating physical properties. Despite significant advances in graphene-like 2D nanosheets, it remains a challenge to explore high-*k* dielectric counterparts, which have great potential in new 2D electronics. Oxide nanosheets may be the perfect solution as a new era unfolds in 2D dielectrics and post-graphene technology. We found that titania- or perovskite-based nanosheets exhibit superior high-k performance (ε_r=210−320) even at thicknesses of a few nanometers (Fig. 1), opening a new route to ultra-scale electronic devices. Notably, nanosheet-based capacitors exhibited an unprecedented capacitance density (~100 μF/cm^2), which was 1,000-fold higher than that of state-of-the-art ceramic condensers. We also utilized high-*k* oxide nanosheets as building blocks in LEGO-like assembly and successfully developed various functional nanodevices such as nanosheet field-effect transistors, all-nanosheet capacitors, artificial ferroelectrics, multiferroics, etc. Our work is a proof-of-concept effort, showing that high-performance nanodevices can be made from "nanosheet architectonics."

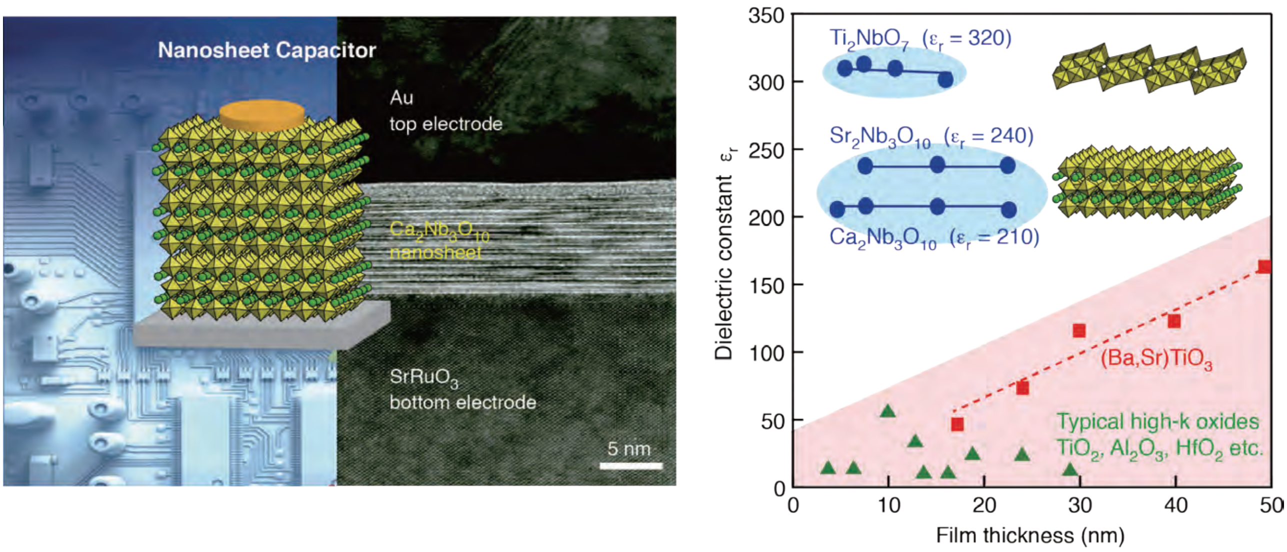

Fig. 1 Schematic illustration and transmission electron microscopic image of a nanosheet-based capacitor (left). Dielectric properties of oxide nanosheets and various oxide thin films (right).

Main Papers

1) "Two-dimensional dielectric nanosheets: Novel nanoelectronics from nanocrystal building blocks", M. Osada, T. Sasaki, *Adv. Mater.* **24** (2012) 210.

2) "All-nanosheet ultrathin capacitors assembled layer-by-layer via solution-based processes", C. Wang, M. Osada, Y. Ebina, B.W. Li, K. Akatsuka, K. Fukuda, W. Sugimoto, R. Ma, T. Sasaki, *ACS Nano* **8** (2014) 2658.

3) "Coexistence of magnetic order and ferroelectricity at 2D nanosheet interfaces", B.W. Li, M. Osada, Y. Ebina, S. Ueda, T. Sasaki, *J. Am. Chem. Soc.* **138** (2016) 7621.

03 High-performance gapless atomic switch and related nanoionic devices

K. Terabe, T. Tsuruoka, T. Tsuchiya, T. Hasegawa, M. Aono

We developed a quantized conductance gapless atomic switch utilizing ion migration. Quantized conductance was observed by controlling an atomic point contact between a metal filament and an electrode in the atomic switch with a simple metal–insulator–metal layered structure. Furthermore, an all-solid-state electric double-layer transistor (EDLT) based on a nanoionic device principle using ion migration was created for electrical modulation of superconducting critical temperature (Tc).

Semiconductor device performance is supported by technological developments for refinement and integration. However, in the not-too-distant future, those developments may halt. To continue upgrading information and communication devices, it is essential to create next-generation nanodevices operating under new principles. We developed a gapless-type atomic switch, following the invention of a gap-type atomic switch for new nanodevices. Field-programmable gate arrays (FPGAs) incorporating numerous gapless atomic switches are near commercialization. The performance of conventional integrated circuits could improve dramatically using FPGAs.

Unique characteristics of the atomic switch allow use in various applications. Atomic switches not only improve the performance of current computing systems using only on/off resistance change but also enable the development of conceptually new electronic systems. The atomic switch allowed the development of multiple-valued nonvolatile memory using quantized conductance. Fig. 1(a) shows the conductance change as pulse biases are applied to the gapless atomic switch with a $Ag/Ta_2O_5/Pt$ structure[1]. Increases and decreases in quantized conductance occur by applying positive and negative pulse biases, which can be used in multiple-valued memory. Furthermore, Tc is modulated by doping high-density carriers in metal film using an all-solid-state EDLT [2,3]. This operation utilizing local ion migration control is derived from the atomic switch principle. The temperature dependence of Nb channel resistance of the EDLT with a $LiCoO_2/Li_4SiO_4/Nb$ structure is plotted in Fig. 1(b). Tc_{zero} values increase from 8.23 to 8.27 K when gate biases are reduced from 2.5 to −2.5 V. This method can be used in searching for novel high-Tc superconductors.

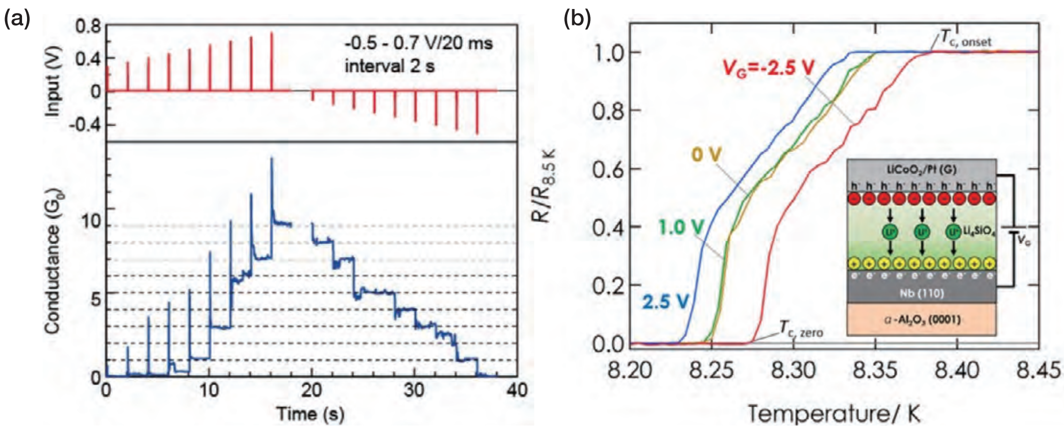

Fig. 1(a) Increase and decrease in quantized conductance by applying positive and negative pulse bias. **(b)** Tc modulation caused by high-density carrier doping using an all-solid-state EDLT.

Main Papers

1) "Conductance quantization and synaptic behavior in a Ta_2O_5-based atomic switch", T. Tsuruoka, T. Hasegawa, K. Terabe, M. Aono, *Nanotechnology* **23** (2012) 435707.
2) "All-solid-state electric-double-layer transistor based on oxide ion migration in Gd doped CeO_2 on $SrTiO_3$ single crystal", T. Tsuchiya, K. Terabe, M. Aono, *Appl. Phys. Lett.* **103** (2013) 073110.
3) "Modulation of superconducting critical temperature in niobium film by using all-solid state electric-double-layer transistor", T. Tsuchiya, S. Moriyama, K. Terabe, M. Aono, *Appl. Phys. Lett.* **107** (2015) 013104.

04 Artificial inorganic synapses achieved using atomic switch technology

T. Tsuruoka, K. Terabe, T. Hasegawa, M. Aono

We demonstrated that atomic switches can emulate the synaptic plasticity underlying memory functions in the human brain. The change in the conductance of the atomic switch is considered analogous to the change in the strength of a biological synapse which varies according to stimulating input pulses. The atomic switch therefore has potential for use as an essential building block for neural computing systems.

In biological systems, there are two types of synaptic plasticity: short-term plasticity (STP), in which changes in synaptic strength last for only a very short time and then it quickly returns to the original state; and long-term potentiation (LTP), in which the enhancement of synaptic strength can last from a few hours to the life of the living organism. The appearance of STP and LTP corresponds to the formation of short-term memory (STM) and long-term memory (LTM), which depends on the strength, frequency, and number of stimuli.

Atomic switches can mimic this synaptic behavior when device conductance varies depending on the repetition rate, amplitude, and number of input voltage pulses (Fig. 1(a)). The STM and LTM behaviors were first discovered in a gap-type Ag_2S atomic switch[1]. For practical applications, the realization of synaptic properties by a gapless-type atomic switch is more important, because it can be easily integrated into complementary metal–oxide–semiconductor (CMOS) circuits. We demonstrated synaptic behavior in an $Ag/Ta_2O_5/Pt$ device based on the transport of metal ions[2]. A temporary increase in conductance and its spontaneous decay over time is observed with lower repetitions of input stimuli, but persistent enhancement is achieved by higher input repetitions, as shown in Fig. 1(b). The transition from STM to LTM over a wide time scale can also be achieved using the transport of oxygen vacancies in a $Pt/WO_{3-x}/Pt$ device (Fig. 1(c))[3].

Our results show that individual atomic switches enable a new functional element suitable for the design of neural systems that can work without the poorly scalable software and preprograming employed in current CMOS-based neural networks. These artificial synapses will contribute to the achievement of next-generation neural computing systems.

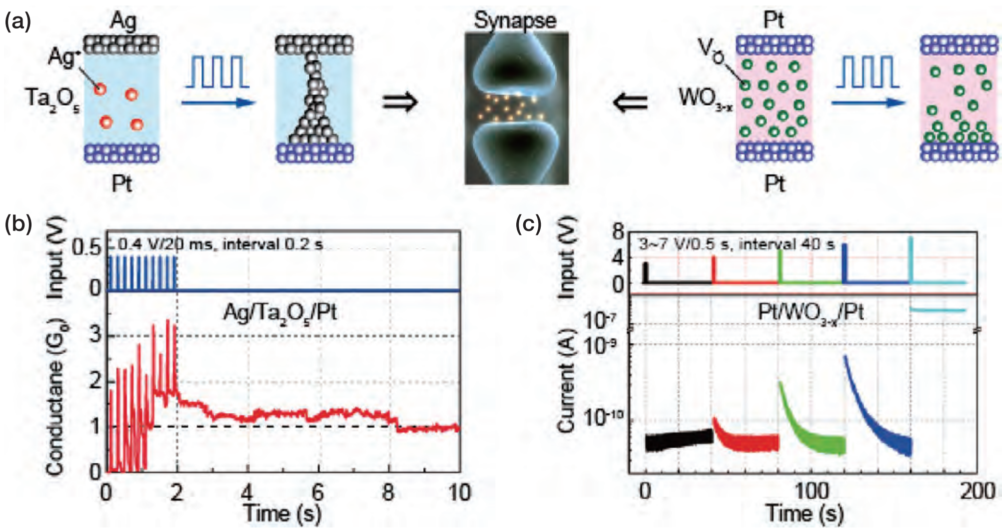

Fig. 1(a) Atomic switches work as an inorganic synapse. **(b)** An Ag/Ta_2O_5-based device shows LTM under high input repetition rates. **(c)** A Pt/WO_{3-x}-based device shows the transition from STM to LTM depending on input strength.

Main Papers

1) "Short-term plasticity and long-term potentiation mimicked in single inorganic synapses", T. Ohno, T. Hasegawa, T. Tsuruoka, K. Terabe, J.K. Gimzewski, M. Aono, *Nat. Mater.* **10** (2011) 591.
2) "Conductance quantization and synaptic behavior of a Ta_2O_5-based atomic switch", T. Tsuruoka, T. Hasegawa, M. Aono, *Nanotechnology* **23** (2012) 435705.
3) "Synaptic plasticity and memory functions achieved in a WO_{3-x}-based nanoionics device by using the principle of atomic switch operation", R. Yang, K. Terabe, Y. Yao, T. Tsuruoka, T. Hasegawa, J.K. Gimzewski, M. Aono, *Nanotechnology* **24** (2013) 384003.

05 Atomic switch networks: nanoarchitectonic design of a neuromorphic system for future computing

J. K. Gimzewski, A. Z. Stieg, M. Aono

Through a conceptual convergence of nanoarchitectonics, neuroscience, and machine learning, we developed hardware-adaptive computing architectures based on deeply hierarchical networks of memristive elements. Atomic switch networks (ASNs) seek to realize revolutionary efficiency, performance, and robustness in high-performance computing by envisioning a new approach to intrinsic computing with target applications in embedded systems, mobile devices, robotics, and autonomous control. ASN devices have been used to demonstrate one of the first hardware implementations of pattern recognition and forecasting tasks without the need for preprogramming.

Transformational advances in computation are needed to address ever-increasing societal demands for the collection, processing, and analysis of large, unstructured, multisensory datasets. Conventional computer hardware is excellent at performing deterministic tasks involving error-free calculations, but it faces fundamental constraints in more complex applications such as autonomous control, pattern recognition, or prediction. In contrast, natural systems autonomously process information in complex environments with extreme energetic efficiency. General-purpose, top-down engineered computing architectures must be redefined to consider dynamic and adaptive systems that process information in novel and scalable ways. Efforts to develop radically new computing paradigms have intensified in recent years, with the technological promise of computation beyond the digital realm for cheaper, faster, more robust, and more energy-efficient information processing.

Emulating the computational performance of natural systems requires new materials, architectures, and conceptual frameworks in which the development of functional nanomaterials integrating memory and information-processing capabilities will support breakthrough research in the design and application of next-generation neurocomputing systems. As shown in Fig. 1, ASN devices comprise individual atomic switch elements embedded within a network of highly interconnected, self-organized nanowires integrated into a complementary metal–oxide semiconductor (CMOS)-compatible device platform[1)].

ASN devices utilize the intrinsic memory capacity and adaptive interactions of functional nanoscale elements, i.e., memristive atomic switches, to generate a class of emergent operational characteristics reminiscent of natural systems[2)] which can be readily applied to real-time information-processing and computational tasks, specifically in the area of reservoir computing[3)]. By successfully implementing a series of real-time computational tasks, ASN devices have achieved their potential utility for information-processing and computing applications. These results will embolden future efforts to develop adaptive computing systems as a means to produce environmental impacts brought about by reduced energy consumption and socioeconomic benefits built upon increased access to actionable information.

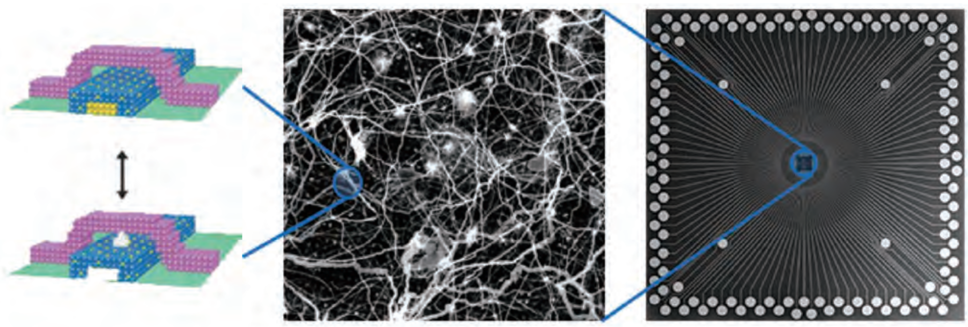

Fig. 1(Left) Schematic representation of a single atomic switch. Center: Scanning electron microscope image of an ASN device comprising individual atomic switch elements embedded within a network of highly interconnected silver wires. **(Right)**Self-organized nanowires integrated into a CMOS-compatible device platform with 120 electrodes[1].

Main Papers

1) "Atomic switch networks: nanoarchitectonic design of a complex system for natural computing," E. Demis, R.C Aguilera, H.O. Sillin, E.J. Sandouk, K. Scharnhorst, M. Aono, A.Z. Stieg, J.K Gimzewski, *Nanotechnology* **26** (2015) 204003.
2) "Emergent criticality in complex Turing B-type atomic switch networks", A.Z. Stieg, A.V. Avizienis, H.O. Sillin, C. Martin-Olmos, M. Aono, J.K. Gimzewski, *Adv. Mater.* **24**(2) (2012) 286.
3) "A theoretical and experimental study of neuromorphic atomic switch networks for reservoir computing," H.O. Sillin, H.H. Shieh, R. Aguilera, A.V. Avizienis, M. Aono, A.Z. Stieg, J.K. Gimzewski, *Nanotechnology* **24**(38) (2013) 384004.

06 Single-molecule-level molecular memories for ultra-high density storage

T. Nakayama, M. Aono Co-workers: M. Nakaya, S. Tsukamoto

Ultrahigh-density data storage has been considered to be one of the important outcomes by utilizing single-molecule manipulation with a scanning tunneling microscope (STM). However, there has been a crucial problem for many years; how to achieve reversible and repeatable control of a molecular bit to represent 0 and 1. We solved this long-standing problem by reversibly controlling bound and unbound states of C_{60} molecules at room temperature, and demonstrated actual bit operations at a bit density of 190 Tbits/in^2.

We used a thin film of fullerene C_{60} molecules and controlled single-molecule-level chemical reaction between C_{60} molecules in the film using an STM tip. We found that negative and positive ionization of a designated C_{60} molecule can selectively trigger polymerization and depolymerization reactions of the designated C_{60} molecule, respectively, with an adjacent molecule in the film. The mechanism of this STM-induced chemical reaction was experimentally and theoretically studied. When the film of C_{60} molecules is negatively biased against an STM tip, electron donation to C_{60} molecules occurs under the tip and the lowest unoccupied molecular orbital (LUMO) of C_{60}, the bound state between C_{60} molecules, is partially occupied. Further electronic excitation by tunneling electrons fulfills the bound state with two electrons, stabilizing the bound C_{60} molecule. When using opposite biases, the bound C_{60} molecules are positively ionized by extraction of electron. The destabilized bound state finally dissolves with the help of electronic excitation by tunneling electrons. Because electronic excitation by STM is in a very confined area, only a single C_{60} molecule underneath the STM tip can be controlled. Bound and unbound states of C_{60} molecules are easily recognized by the appearance and disappearance of depression of the film, and we demonstrated ultradense data storage at a bit density of 190 Tbits/in^2 by controlling the chemical reactions at a single-molecule precision as shown in Fig. 1.

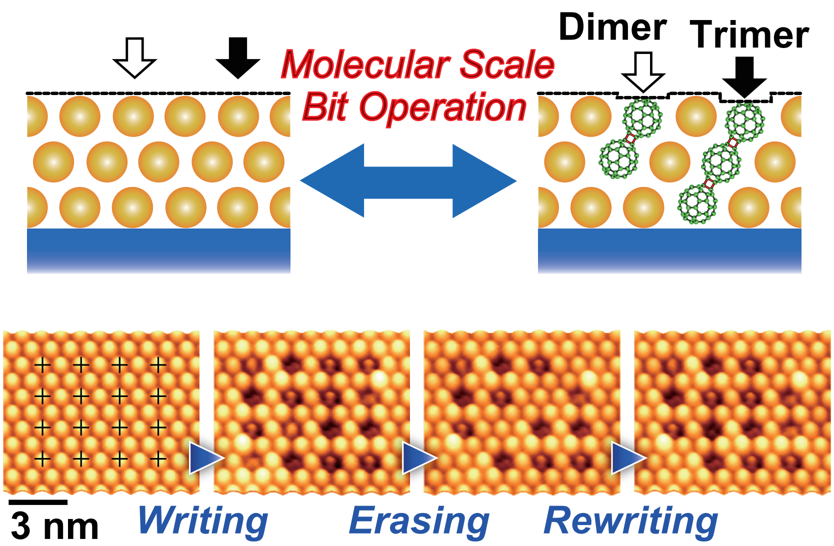

Fig. 1 Schematic illustration of local and reversible control (equivalent to bit operation)of bound and unbound states of C_{60} molecules (top). A series of STM images showing single-molecule-level bit operation achieved by this technique

Main Papers

1) "Molecular-scale control of unbound and bound C_{60} for topochemical ultradense data storage in an ultrathin C_{60} film", M. Nakaya, S. Tsukamoto, Y. Kuwahara, M. Aono, T. Nakayama, *Adv. Mater.* **22** (2010) 1622.
2) "Molecular-scale size tuning of covalently bound assembly of C_{60} molecules", M. Nakaya, M. Aono, T. Nakayama, *ACS Nano* **5** (2011) 7830.
3) "Ultrahigh-density data storage into thin films of fullerene molecules", M. Nakaya, M. Aono, T.Nakayama: Jpn. *J. Appl. Phys.* **55**, 1102B4 (2016).

07 Molecular wiring and single-molecular devices

Y. Okawa, M. Aono
Co-workers: Y. Tateyama, C. Joachim, M. Makarova, E. Verveniotis

We developed a novel method for single-molecular wiring using nanoscale-controlled chain polymerization on a molecular layer. This method, which we call "chemical soldering," enables us to connect single conductive polymer chains to single functional molecules via covalent bonds. We are investigating the electrical transport properties of the fabricated single-molecular devices. These studies will be an important step in advancing the development of single-molecule electronic circuitry.

Although single-molecule electronics have been widely investigated for a long time, the fabrication of practical single-molecule circuits remains challenging because of the lack of viable methods for wiring each molecule. We previously found that stimulation with the tip of a scanning tunneling microscope (STM) on a molecular layer of a diacetylene compound could initiate chain polymerization of the molecules. As a result, we could fabricate a single conductive polydiacetylene (PDA) chain at designated positions. Based on the previous results, we developed a novel method for connecting single conductive polymer chains to single organic molecules[1,2]. Fig. 1(a) shows a schematic illustration of the wiring procedure. First, the relevant functional molecules are placed on a self-assembled monolayer of a diacetylene compound. The STM tip is then positioned on the molecular row to which the functional molecule is adsorbed, and a conductive PDA chain (shown as yellow lines in Fig. 1(a)) is fabricated by initiating chain polymerization. Since the front edge of chain polymerization necessarily has a reactive chemical species, the polymer chain created forms covalent bonds with a molecular elements encountered. We call this spontaneous reaction "chemical soldering."

We demonstrated that two PDA chains are connected to a single phthalocyanine (Pc) molecule (Fig. 1(b)). First-principles theoretical calculations, together with the detailed analysis of STM images, were used to investigate the structures and electronic properties of the connection. The estimated electronic states predict that the fabricated PDA–Pc–PDA system will act as a resonant tunneling diode (Fig. 1(c)). We are investigating the electrical transport properties of the devices fabricated on insulating substrates[3], such as hexagonal boron nitride or functionalized graphene substrates. These studies will be an important step in advancing the development of single-molecule electronic circuitry, which will help us to fabricate novel, extremely small devices with low energy consumption.

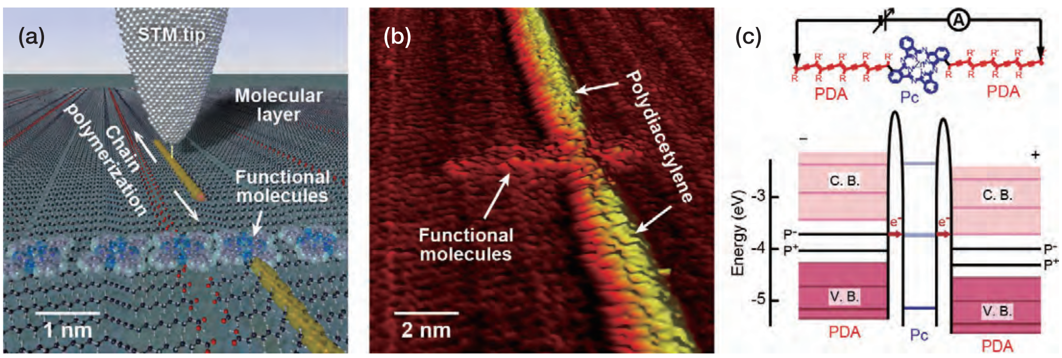

Fig. 1(a) Schematic illustration and **(b)** STM image of chemical soldering. Chain polymerization is initiated with the STM tip. Two PDA chains are connected to a single functional molecule (Pc). **(c)** Energy level diagram of the PDA–Pc–PDA system showing possible application to resonant-tunneling diodes. When the bias voltage is adjusted so that the energy of the polaron state of PDA (P^+ and P^-) is equivalent to the energy level of Pc, electrons can flow through Pc.

Main Papers

1) "Chemical wiring and soldering toward all-molecule electronic circuitry," Y. Okawa, S.K. Mandal, C. Hu, Y. Tateyama, S. Goedecker, S. Tsukamoto, T. Hasegawa, J.K. Gimzewski, M. Aono, *J. Am. Chem. Soc.* **133** (2011) 8227.

2) "Controlled chain polymerisation and chemical soldering for single-molecule electronics," Y. Okawa, M. Akai-Kasaya, Y. Kuwahara, S.K. Mandal, M. Aono, *Nanoscale* **4** (2012) 3013.

3) "Self-assembled diacetylene molecular wire polymerization on an insulating hexagonal boron nitride (0001) surface," M.V. Makarova, Y. Okawa, E. Verveniotis, K. Watanabe, T. Taniguchi, C. Joachim, M. Aono, *Nanotechnology* **27** (2016) 395303.

08 Design of molecular quantum mechanical logic gates

C. Joachim, S. Srivastava, H. Kino

Based on quantum Hamiltonian computing (QHC), we have designed a 2-nm single-molecule ½ adder with 4 planar graphene nanopads. This molecule runs Boolean calculations with quantum-level repulsion, optimized destructive interference, and only 4 of its molecular electronic states. The QHC classical to quantum 2-input conversion is ensured by the rotation of two nitro chemical groups that can be activated by the tip of a scanning tunneling microscope (STM). From 0.1 to 2 μA, the ½ adder XOR and AND output currents are measured at the same low bias voltage.

As shown in Fig., the QHC calculating molecule is bonded to 4 ultra-short nanoribbons, each bonded to a semi-infinite graphene nanopad. Oriented in the same atomic direction as the nanopads, those nanoribbons define the measuring quantum pointer states. This planar measuring circuit can be nanofabricated using high-precision He+ scattering and single C-atom STM vertical manipulations. The A and B nitro inputs are chemically bonded to the calculating molecule. A planar nitro encodes for a "0" and a perpendicular nitro for a "1" logical input. The logical input quantum information is distributed among the XOR and AND parts with no ancillary molecular wires and no cloning of quantum information. To calculate, the central molecule manipulates the quantum information encoded in its electronic eigenstates which is modified by the nitro rotations. This is the practical implementation of our formal QHC ½ adder[1].

Starting from classical inputs and to run a quantum calculation, QHC benefits from the spontaneous time-dependent Heisenberg-Rabi quantum oscillations of the molecule prepared in a non-stationary electronic state[1]. By measuring the corresponding secular oscillation frequency with a pair of graphene nanopads per output, Boolean operations are performed in parallel. A QHC NOR gate molecule was already experimentally demonstrated based on a single tri-naphthalene molecule physisorbed on an Au(111) surface[2].

The measured XOR and AND output current intensities were calculated using the multichannel electronic transparency between any nanopad couple and the scattering matrix calculated exactly using a full-valence Slater basis set based on the elastic scattering quantum chemistry (N-ESQC) theory[3]. The Boolean logical quantum circuit performance is presented in Fig, demonstrating how a complex Boolean logic function can be realistically designed in a carbon monolithic approach. There is no need to divide the central calculating molecule into parts using molecular wires, switches, rectifiers, transistors, or qubits.

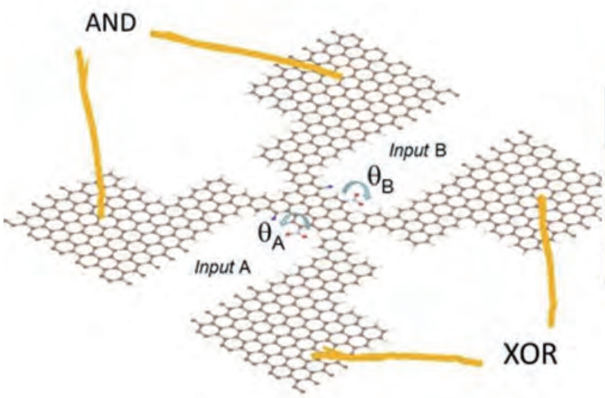

Input A	Input B	Rotation angle θ_A	Rotation angle θ_B	XOR output /μA	AND output /μA	XOR	AND
0	0	0°	0°	1.7×10^{-6}	0.1×10^{-4}	0	0
0	1	0°	90°	0.062	0.74×10^{-4}	1	0
1	0	90°	0°	0.062	0.74×10^{-4}	1	0
1	1	90°	90°	8.7×10^{-4}	2.01	0	1

Fig. 1 The QHC ½ adder calculating molecule with its 2 nitro chemical group classical inputs and its 4 graphene-contacting nanopads with the table of the N-ESQC calculated logical performance (*Chem. Phys. Lett.*, DOI/10.1016/j.cplett.2016.11.009).

Main Papers

1) "The mathematics of a QHC ½ adder Boolean logic gate", G. Dridi, R. Julien, M. Hliwa, C. Joachim, *Nanotechnology* **26** (2015) 344003.
2) "Manipulating molecular quantum states with classical metal atom inputs: demonstration of a single molecule NOR logic gate", W.H. Soe, X. Manzano, N. Renaud, P. De Mandoza, A. De Sarkar, F. Ample, M. Hliwa, A.M. Echevaren, N. Chandrasekhar, C. Joachim, *ACS Nano* **5** (2011) 1436.
3) "Molecular OR & AND logic gates integrated in a single molecule", S. Ami, M. Hliwa, C. Joachim, *Chem. Phys. Lett.* **367** (2003) 662.

09 Multiple-probe scanning probe microscopes for material nanoarchitectonics

T. Nakayama, Y. Shingaya, O. Kubo, M. Aono

The novel properties of individual nanostructures and nanosystems, the outgrowth of material nanoarchitectonics, must be characterized using innovative instruments and methodologies. For this purpose, we developed multiple-probe scanning probe microscopes (MP-SPMs) and thus created a new class of nanoscale measurements enabling us to perform unique, indispensable nanomeasurements.

MP-SPMs equipped with two to four individually driven probes are used for imaging nanostructures of interest and for performing multiprobe electrical measurements by direct contact between the same probes and a single nanostructure or a nanoarchitectonic nanosystem (Fig. 1). For example, a single-walled carbon nanotube (SWCNT) on SiO_2 was imaged by two probes of a multiple-probe scanning tunneling microscope, and the length of the electron mean-free-path of the SWCNT was directly measured to be about 500 nm at room temperature (Fig. 1). A multiple-probe atomic force microscope (MP-AFM) using newly developed tuning fork sensors was also developed, and this MP-AFM enabled measurements of conductive nanostructures on insulating substrates. High-resolution imaging of an object to be measured, precisely controlled and reproducible point-contact formation, and accurate interprobe distance estimation are all indispensable advantages of MP-SPMs compared with other characterization methods. In addition, MP-SPM measurements require neither preprocessing of samples such as electrode formation by lithographic processes nor scanning electron microscope observation. This is often crucial to avoid damage to and changes in nanoscale objects. We have recently implemented a noncontact potential mapping function (Kelvin probe force microscopy [KFM]) in our MP-AFM. In general, quadruple-probe measurements prevent the effects of contact resistance when an area sufficiently larger than the interprobe distance is dealt with. Our MP-AFM can perform not only quadruple-probe measurements at the nanometer scale but also contact-free electrical measurements using two AFM probes for flowing a current through a target object and one KFM probe to map potential variation over the object. This feature is extremely important when characterizing nanoarchitectonic systems achieved through material nanoarchitectonics because such systems should exhibit structural and functional variation over the entire system.

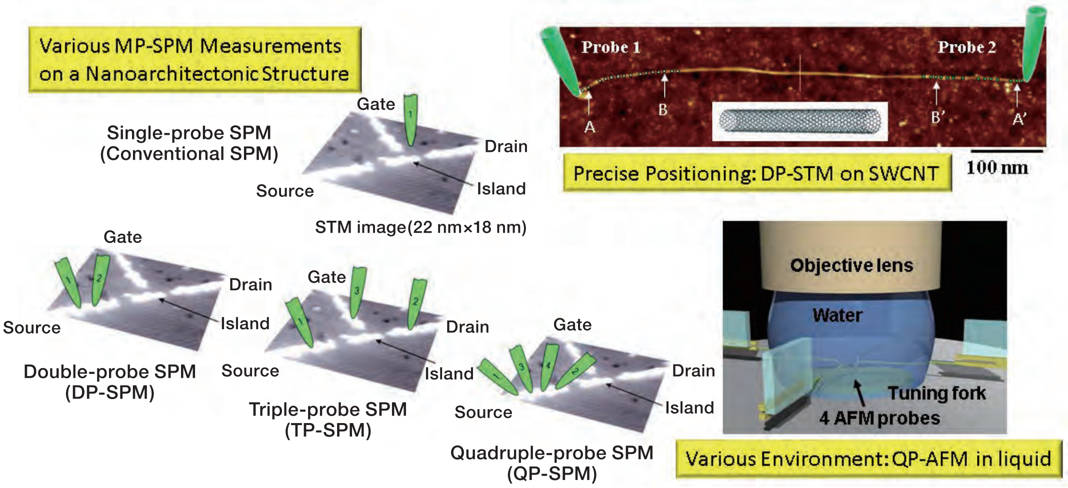

Fig. 1 Left: MP-SPMs enabling various types of nanoscale measurements. Upper right: Example of double-probe SPM measurement carried out for an SWCNT. Lower right: Instrumentation of a quadruple-probe SPM for material nanoarchitectonics in a liquid environment.

Main Papers

1) "Development and application of multiple-probe scanning probe microscopes", T. Nakayama, O. Kubo, Y. Shingaya, S. Higuchi, T. Hasegawa, C.-S. Jiang, T. Okuda, Y. Kuwahara, K. Takami, M. Aono, *Adv. Mater.* **24** (2012) 1675.
2) "Quadruple-scanning-probe force microscope for electrical property measurements of microscopic materials", S. Higuchi, O. Kubo, H. Kuramochi, M. Aono, T. Nakayama, *Nanotechnology* **22** (2011) 285205.
3) "Multiple-probe scanning probe microscopes for nanoarchitectonic materials science", T. Nakayama, Y. Shingaya, M. Aono, *Jpn. J. Appl. Phys.* **55** (2016) 1102A7.

10 Pioneering development of *in situ* transmission electron microscope techniques for direct property measurements on nanoscale materials

D. Golberg, N. Kawamoto, M. Mitome, Y. Bando

State-of-the-art *in situ* analytical methods of nanomaterial property measurements inside a high-resolution transmission electron microscope (TEM) were for the first time designed and implemented for mechanical, electrical, thermal, optical, optoelectronic, and cathodoluminescence characterizations of various nanoscale nitrides, oxides, sulfides, selenides, phosphides, and carbides. Clear atomic structure–functional property relationships were established, which is the "Holy Grail" of the material "nanoarchitectonics" concept and the entire material science field.

Unprecedentedly high spatial (down to 60 pm), energy, and temporal resolution capabilities, only achievable in the most modern high-resolution TEMs, were greatly enriched by adding new possibilities for delicate nanomanipulations (with precision better than 1 nm) and electromechanical, thermal, and optical probing of diverse nanostructures using piezo-driven stages and optical fibers inserted into a TEM column. Temperature gradients along and across carbon nanotube electrical interconnects under resistive heating were elucidated for the first time[1]. The quantitative kinetics of the famous Nobel Prize-winning "Scotch tape" technique for making graphenes, and of various inorganic atomically thin nanosheets in booming layered semiconductors were fully understood, taking the example of molybdenum disulfide single-crystal direct nanoscale peeling in a TEM[2]. Young's modulus, tensile strength, and fracture toughness of carbon, boron nitride, and tungsten disulfide nanotubes and nanosheets, and silicon, zinc oxide, and sulfide, and gallium nitride nanowires were directly and unambiguously measured for the first time[3]. World-first *in situ* TEM optoelectronic and photovoltaic tests of the most popular optical materials, e.g., cadmium sulfide, titanium oxide, zinc oxide, silicon, and various perovskites, were performed and specific optoelectronic characteristics were completely understood in terms of their nanomaterial local crystallography and atomically and chemically resolved interfaces, as well as defect structures.

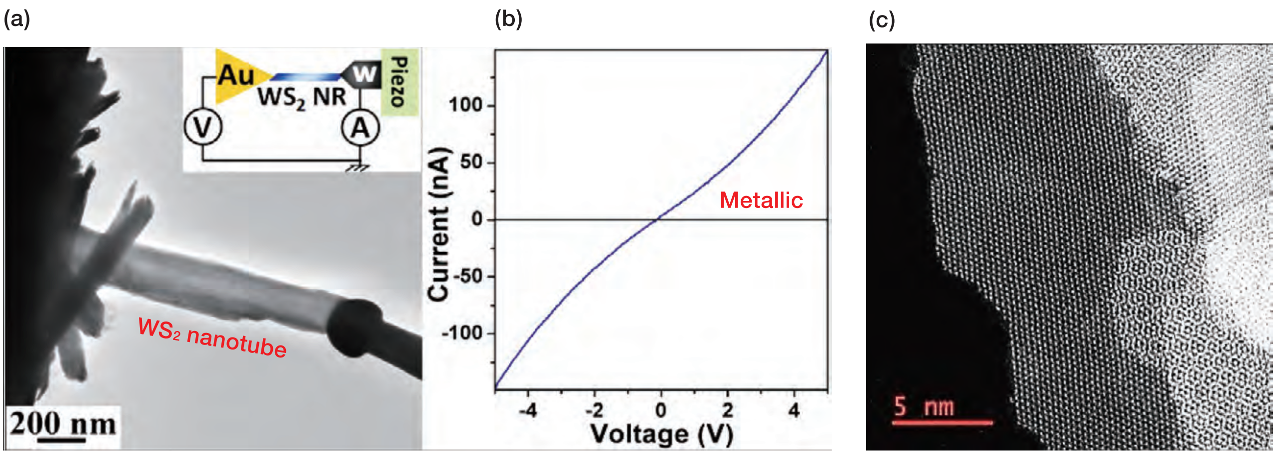

Fig. 1 **(a)**Low-magnification TEM view of the assembled *in situ* setup featuring an individual tungsten disulfide nanotube stretched and electrically tested between the two metal electrodes; and **(b)** a corresponding metallic type I-V curve directly recorded from it in TEM. **(c)** High-angle annular dark-field TEM image of a peeled (inside the TEM) molybdenum disulfide atomically thinnest flake (each bright spot represents an individual Mo atom) showing a monoatomic edge domain on the left and striking moiré patterns on the right due to overlapped and shuffled atomic layers.

Main Papers

1) "Direct imaging of Joule heating dynamics and temperature profiling inside a carbon nanotube interconnect", P.M.F.J. Costa, U.K. Gautam, Y. Bando, D. Golberg, *Nat. Commun.* **2** (2011) 421.
2) "Nanomechanical cleavage of molybdenum disulfide atomic layers", D.M. Tang, D.G. Kvashnin S. Najmaei, Y. Bando, K. Kimoto, P. Koskinen, P.M. Ajayan, B.I. Yakobson. P.B. Sorokin, J. Lou, D. Golberg, *Nat. Commun.* **5** (2014) 3631.
3) "Nanomaterial engineering and property studies in a transmission electron microscope", D. Golberg, P.M.F.J. Costa, M.S. Wang, X.L. Wei, D.M. Tang Z. Xu, Y. Huang, U.K. Gautam, B.D. Liu, H. Zeng, N. Kawamoto, C.Y. Zhi, M. Mitome, Y. Bando, *Adv. Mater.* **24** (2012) 177.

11 Nanomechanical sensing technologies (MSS, AMA) for olfactory sensor systems

G. Yoshikawa, K. Shiba Co-worker: G. Imamura

We developed novel nanomechanical sensing technologies, the Membrane-type Surface stress Sensor (MSS) and Aero-Thermo-Dynamic Mass Analysis (AMA). The comprehensive structural optimization and integration of nanomaterials as receptors led to the unique MSS structure with much higher sensitivity, stability, and compactness compared with conventional nanomechanical sensors. AMA enables nanoarchitectonic analyses of the fundamental properties (molecular weight) of gas samples under ambient conditions.

The demand for new sensors to detect or identify target molecules is growing rapidly in fields such as food, agriculture, medicine, security, and the environment. Nanomechanical sensors have the potential to meet this global demand owing to their intrinsic versatility. To move toward practical applications that require both sensitivity and compactness, the MSS (Fig. 1 (a))[1] was developed through the comprehensive optimization of technologies in various relevant fields, such as material science, mechanics, crystallography, and electronics, in collaboration with the late Dr. Heinrich Rohrer and the micro-electromechanical team at the École Polytechnique Federale de Lausanne. The unique structure of the MSS achieved >100-fold higher sensitivity in addition to better performance in various practical aspects, such as smaller size, higher reproducibility, higher mechanical and electrical stability, and simpler operation. The integration of nanoparticle-based materials as receptors enhances the sensitivity even further with flexible chemical selectivity.

While the MSS provides a practical sensing element, a consumer sensor system requires further optimization and integration of many components including various receptor layers, hardware including electronics and sample handling, multidimensional data analysis, and precise calibration for high reproducibility. To establish a *de facto* standard for odor analysis and sensor systems employing the nanomechanical MSS technology, the MSS Alliance was launched jointly with companies and a university[2].

The MSS measures rather relative properties of gas samples, while measurements of the absolute aspect of each gas can allow comprehensive characterization. AMA (Fig. 1(b))[3] was developed as a novel approach to the direct measurement of the fundamental properties of gases (molecular weight) through a nanoarchitectonic combination of aerodynamics, thermodynamics, and mechanics, transducing microscopic events into macroscopic phenomena. Since AMA directly measures molecular weight under ambient conditions without a vacuum or ionization, it can be integrated into analytical devices, production lines, and consumer mobile platforms.

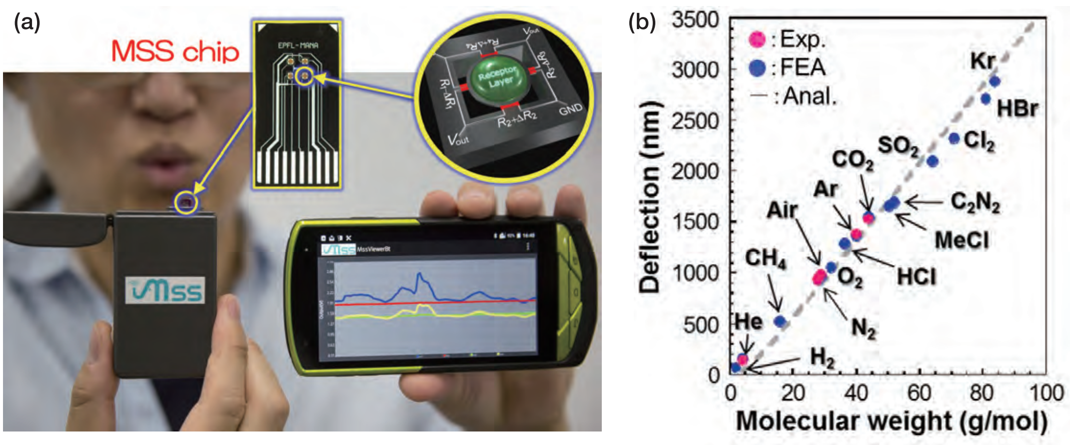

Fig. 1(a) Prototype of a mobile olfactory sensor device based on MSS technology. **(b)** Relationship between molecular weight and deflection measured by AMA.

Main Papers

1) "Nanomecanical membrane-type surface stress sensor", G. Yoshikawa, T. Akiyama, S. Gautsch, P. Vettiger, H. Rohrer, *Nano Lett.* **11** (2011) 1044.
2) "MSS alliance launched to set de facto standard for odor-sensing systems", http://www.nims.go.jp/eng/news/press/2015/10/201510130.html.
3) "Aero-thermo-dynamic mass analysis", K. Shiba, G. Yoshikawa, *Scientific Reports* **6** (2016) 28849.

12 Cathodoluminescence and electron beam-induced current characterization for nanomaterials and devices

T. Sekiguchi, J. Chen Co-workers: K. Watanabe, Y. Cho

Nanoscale observations of material function, such as electrical and/or optical properties, are indispensable for nanoscience and nanotechnology. Thus, we developed scanning electron microscopy (SEM) and improved cathodoluminescence (CL) and electron beam-induced current (EBIC) techniques as well as secondary electron (SE) imaging[1-3].

Modern computer technology demands high electron-mobility transistors (HEMTs) operating at a higher frequency than that of a conventional Si metal–oxide–semiconductor field-effect transistor. The i-GaInAs/n-AlGaAs heterojunction is a promising candidate for the HEMT electron channel structure. However, heteroepitaxial growth may introduce various crystalline defects, which degrade the performance of the electron channel. As part of an EBIC/CL study of the GaInAs channel on an InP substrate, we developed a probe-EBIC system where micromanipulators are installed in an SEM chamber to drive individual metal probes for in-situ local contact (Fig. 1(a)). This probe-EBIC system enables study of the intrinsic properties of GaInAs electron channel structures and the spatial distribution of electrically active defects around the structures on the nano-to-macroscopic scale.

A cross-sectional SE and EBIC images of the heterojunction on InP (001) substrate are shown in Fig. 1(b, c) with an electron beam of 15 keV and 4.4 nA.[3] Apart from the cross-section roughness and related contrasts, there was no dark EBIC contrast around the GaInAs electron channel, meaning that electrically active defects are not present in this channel area. The combination of CL (d) gives much more information about the band structure of this system.

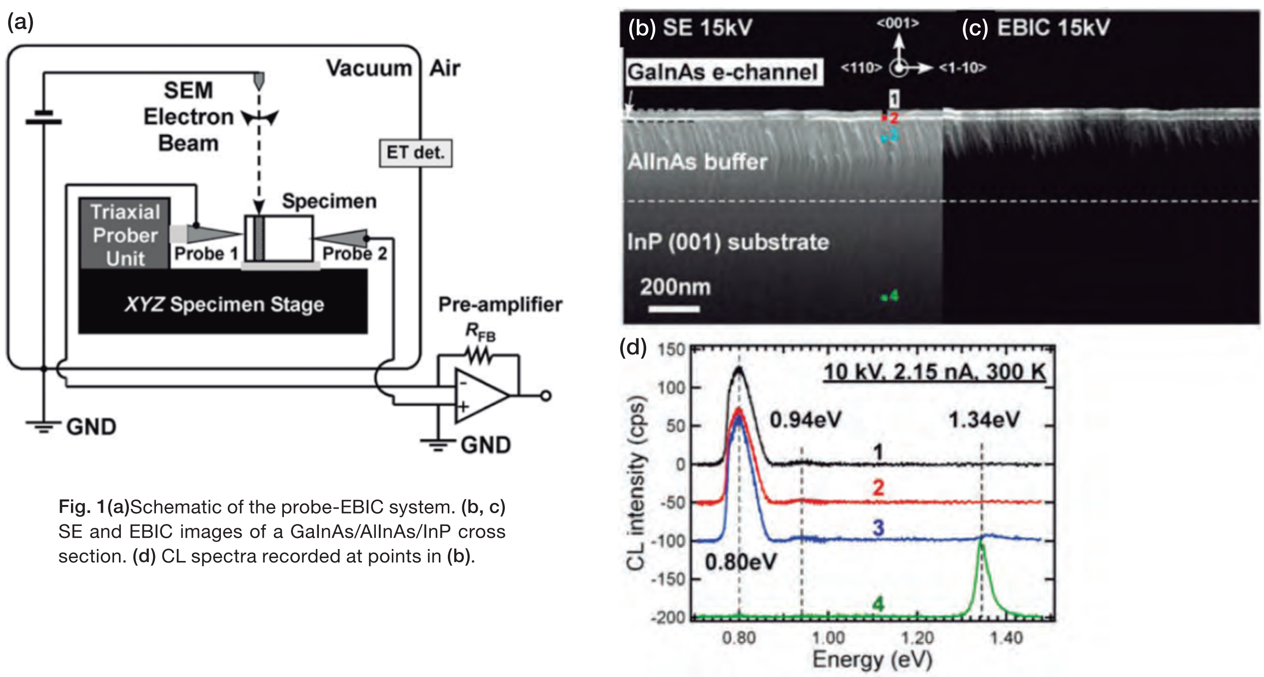

Fig. 1 **(a)** Schematic of the probe-EBIC system. **(b, c)** SE and EBIC images of a GaInAs/AlInAs/InP cross section. **(d)** CL spectra recorded at points in **(b)**.

Main Papers

1) "Arbitrary cross-section SEM-cathodoluminescence imaging of growth sectors and local carrier concentrations within micro-sampled semiconductor nanorods", K. Watanabe, T. Nagata, S. Oh, Y. Wakayama, T. Sekiguchi, J. Volk, Y. Nakamura, *Nat. Commun.* **7** (2016) 10609.
2) "Investigation of dislocations in Nb-doped SrTiO3 by electron-beam-induced current and transmission electron microscopy", J. Chen, T. Sekiguchi, J.Y. Li, S. Ito, W. Yi, A. Ogura, *Appl. Phys. Lett.* **106** (2015) 102109.
3) "Local electrical properties of n-AlInAs/i-GaInAs electron channel structures characterized by the probe-electron-beam-induced current technique", K. Watanabe, T. Nokuo, J. Chen, T. Sekiguchi, *Microscopy* **63** (2012) 161.

II

Fusion of Interdisciplinary Research Fields

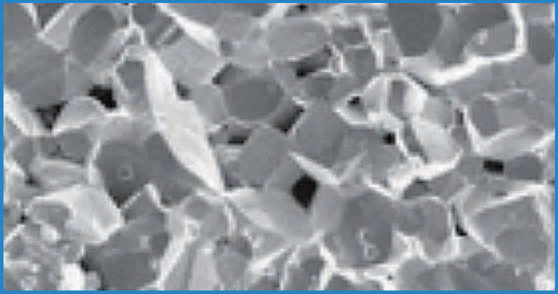
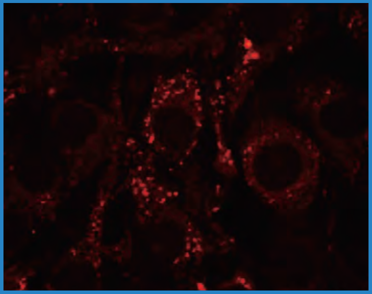
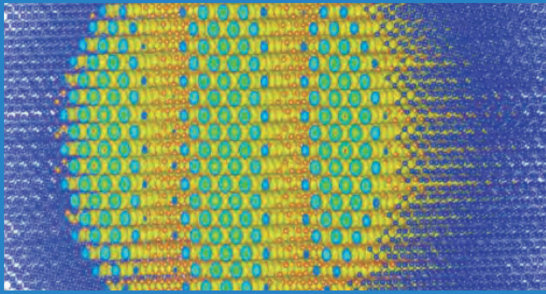

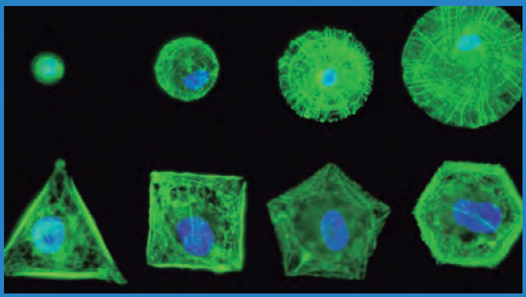

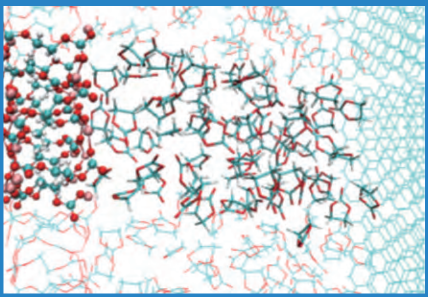

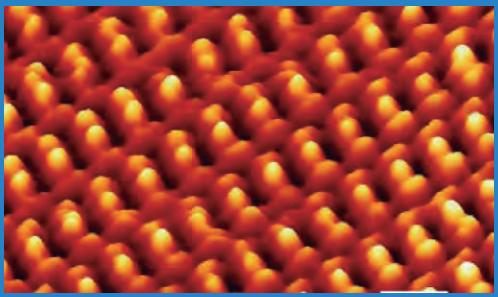

13 Smart nanofibers for cancer therapy

M. Ebara, T. Aoyagi Co-worker: K. Uto

We developed a smart anticancer nanofiber that is capable of simultaneously performing thermotherapy and chemotherapy for treating malignant tumors. By tailoring the nanoarchitectures of polymer networks in the fiber, we demonstrated simultaneous heat generation and drug release in response to an alternating magnetic field (AMF). A 5–10-min application of AMF alone successfully induced cancer apoptosis in both *in vitro* and *in vivo* studies.

Squamous cell carcinoma is an epithelial malignant tumor found in mucous membranes lined by stratified squamous epithelium and in the skin. At present, the main therapeutic methods are surgery, radiation therapy, and chemotherapy, according to the cancer stage. In recent years, thermotherapy (or hyperthermia), which takes advantage of the fact that cancer cells are more sensitive to heat than normal cells, has attracted widespread attention. Since thermotherapy is also effective for enhancing drug efficacy and relieving pain, there are high expectations of its combined use with chemotherapy and other treatments. In this research, we developed a mesh material that can be applied directly to the affected site and is capable of simultaneously performing thermotherapy and chemotherapy for treating epithelial malignant tumors. The nanofiber is composed of a chemically crosslinkable, temperature-responsive polymer combined with an anticancer drug and magnetic nanoparticles (MNPs), which serve as a trigger of drug release and a source of heat, respectively. By tailoring the nanoarchitectures of polymer networks in the fiber, the nanofiber mesh shows switchable changes in the swelling ratio in response to alternating "on-off" switches of the AMF because the self-generated heat from the incorporated MNPs induces the deswelling of polymer networks in the nanofiber. Correspondingly, the on-off release of drug from the nanofibers is observed in response to the AMF. Both *in vitro* and *in vivo* studies showed that the majority of tumor cells died after only a 5–10-min AMF application due to the double effects of heat and drug.

(a)

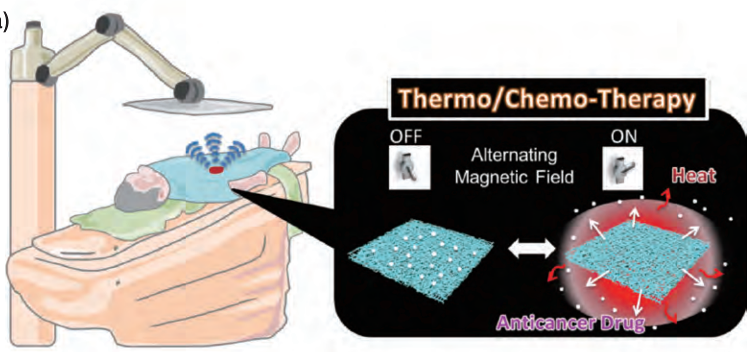

(b)

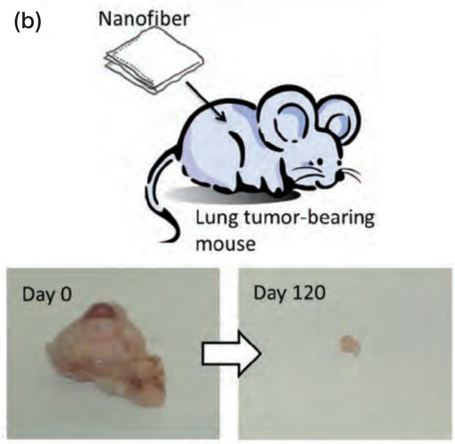

Fig. 1 **(a)** Schematic image of combined thermo/chemotherapy using a smart anticancer nanofiber mesh. **(b)** The nanofiber mesh was implanted on lung tumor-bearing mice that were then subjected to AMF irradiation for 15 min once weekly.

Main Papers

1) "A smart nanofiber web that captures and release cells", Y.-J. Kim, M. Ebara, T. Aoyagi, *Angew. Chem. Intl. Ed.* **51** (2012) 10537.
2) "A smart hyperthermia nanofiber with switchable drug release for inducing cancer apoptosis", Y.-J. Kim, M. Ebara, T. Aoyagi, *Adv. Func. Mater.* **23** (2013) 5753.
3) "Biodegradable nanofiber for delivery of immunomodulating agent in the treatment of basal cell carcinoma", R. Garrett, E. Niiyama, Y. Kotsuchibashi, K. Uto, M. Ebara, *Fibers* **3** (2015) 478.

14 Novel antioxidative nanomedicine for Alzheimer's disease

Y. Nagasaki

Excessively generated reactive oxygen species (ROS) are associated with age-related neurodegenerative diseases including Alzheimer's disease (AD). We investigated whether scavenging of ROS in the brain by orally administered redox nanoparticles (RNPs) facilitates the recovery of cognition in 17-week-old senescence-accelerated-prone mice. After treatment for 1 month, levels of oxidative stress in the brains of the mice were remarkably reduced by treatment with RNPs compared with those in mice treated with low-molecular-weight (LMW) nitroxide radicals, resulting in the amelioration of cognitive impairment with increased numbers of surviving neurons. Additionally, treatment with RNPs did not show any detectable toxicity.

Aging increases the risk of neurodegenerative diseases such as AD, which mostly affect quality of life in the elderly. Although the average human life span has increased because of progress in medicine and healthcare, the socioeconomic burden of the elderly is a concern in developed countries. Oxidative stress caused by overproduction of ROS is a well-known direct cause of aging. Under normal physiological conditions, ROS are scavenged by endogenous antioxidant-defense systems including superoxide dismutase, catalase, and glutathione peroxidase. With advancing age, however, the production of ROS dramatically increases, and endogenous antioxidants fail to scavenge all ROS completely, followed by production of oxidative components. An increase in oxidative stress in the brain is reported to be involved in aging-related neural dysfunction and/or learning and memory deficiency. Although the promising LMW antioxidant vitamin E was reported to show slight efficacy such as slowing of functional decline in clinical trials in AD, complete recovery was not observed. Since the LMW antioxidants internalize easily in healthy cells and disturb important redox reactions such as the electron transport chain, their effective dosage cannot be administered. To prevent such adverse effects of antioxidants, we designed a novel polymer antioxidant (Fig. 1). The amphiphilic character of the polymer antioxidant forms core-shell-type nanoparticles (RNPs), which prevents internalization in healthy cells and markedly decreases undesired adverse effects. After oral administration of RNPs, they disintegrate in the stomach and internalize in the blood stream via the mesentery. The antioxidative polymers finally scavenge ROS in the brain and ameliorate brain dysfunction. On the basis of these results, our antioxidative nanomedicine is promising for new dementia therapeutics including AD.

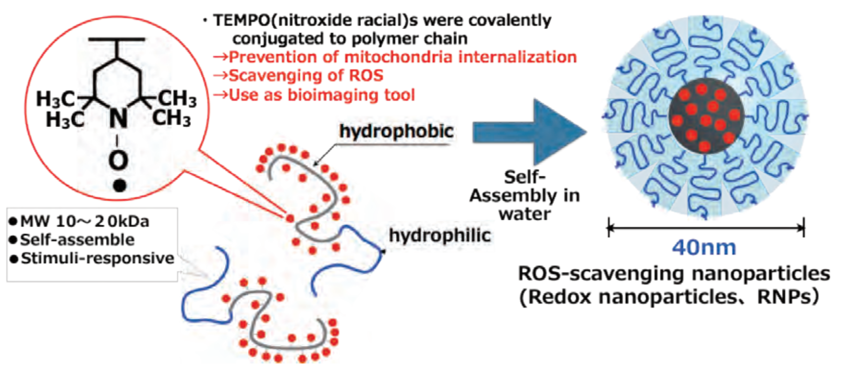

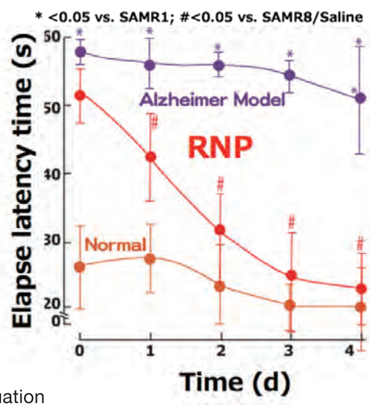

Fig. 1 Design of the antioxidative nanomedicine (left) and evaluation of spatial learning and memory function in Morris water maze tests.

Main Papers

1) "Recovery of cognitive dysfunction via orally administered redox-polymer nanotherapeutics in SAMP8 mice", P. Chonpathompikunlert, T. Yoshitomi, L.B. Vong, N. Imaizumi, Y. Ozaki, Y. Nagasaki, *PLoS One* **10** (2015) e0126013.
2) "The use of nitroxide radical-containing nanoparticles coupled with piperine to protect neuroblastoma SH-SY5Y cells from Aβ-induced oxidative stress", C. Pennapa, T. Yoshitomi, H. Junkyu, H. Isoda, Y. Nagasaki, *Biomaterials* **32** (2011) 8605.
3) "Design of core-shell-type nanoparticles carrying stable radicals in the core", T. Yoshitomi, D. Miyamoto, Y. Nagasaki, *Biomacromolecules* **10** (2009) 596.

15 Photoactivating surfaces to resolve mechanoarchitectonics in collective cell migration

J. Nakanishi

Collective cell migration plays critical roles in various physiological and pathological processes. Therefore, understanding its regulatory mechanisms is important from both fundamental and applied biology viewpoints. We developed a photoactivatable gel substrate as a robust platform for resolving mechanoarchitectonics in collective cell migration.

Recent studies have demonstrated the involvement of physical force in various biological processes, leading to the new discipline "mechanobiology." Cell migration, an essential cellular activity coupling biological reactions to locomotion, is dictated by mechanical and biochemical cues in extracellular environments. Nevertheless, most conventional *in vitro* cell migration assays use plastic plates, which are far stiffer than physiological tissues. Such non-physiological platforms may alter migrating phenotypes and obscure the role of cell migration in physiological and pathological processes.

We developed a robust platform for studying the mechanobiology of collective cell migration. Polyacrylamide gel was used as a soft substrate, with the surface functionalized by photocleavable poly (ethylene glycol). Young's modulus of the substrate was tuned close to *in vivo* soft tissues, while the photoactivatable feature allowed analysis of migration behaviors of geometrically controlled cell clusters by spatiotemporally controlled irradiation of the surface (Fig. 1). Precise geometrical control of cell clusters is important for collective migration studies because traction stress distribution, the major driving force of collective migration, varies depending on cluster geometry as well as substrate stiffness.

Two gel substrates with different stiffness plus a glass control were prepared and collective migration behaviors of epithelial cells on them were analyzed. Quantitatively and qualitatively different collective behaviors were seen depending on material stiffness and migration configuration. However, migration behaviors were almost identical when the cells were seeded as isolated single cells. These strongly suggest that the difference in collective migration behaviors is due to emerging mechanical sensitivity when the cells become a group. This physiologically relevant migration assay platform will be useful for both basic studies of mechanoarchtectonics in collective cell migration and for discovering new drugs regulating cell migration and blocking tumor expansion.

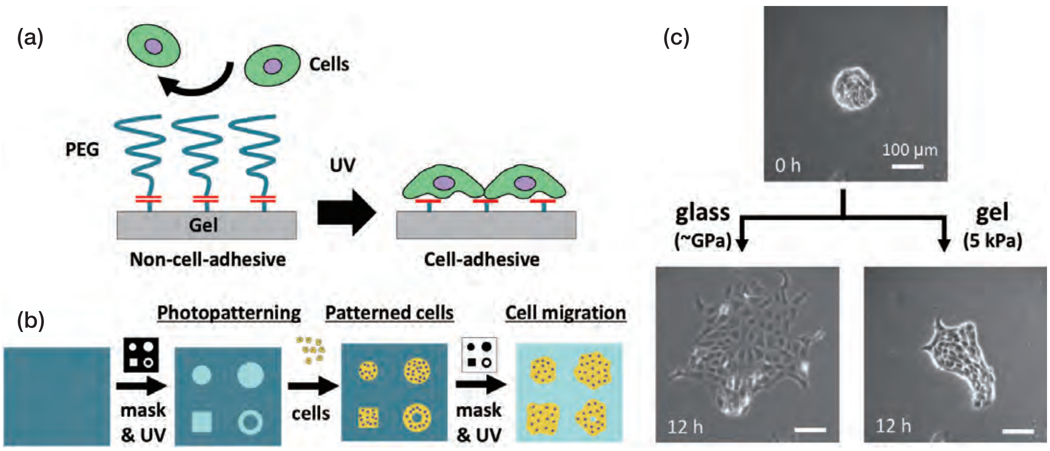

Fig. 1(a) Schematic representation of the photoactivatable gel substrate. **(b)** Procedure for collective cell migration study. **(c)** Different collective behaviors of epithelial cells depending on substrate stiffness.

Main Papers

1) "Dynamic control of cell adhesion on a stiffness-tunable substrate for analyzing the mechanobiology of collective cell migration", M. Kamimura, M. Sugawara, S. Yamamoto, K. Yamaguchi, J. Nakanishi, *Biomater. Sci.* **4** (2016) 933.
2) "Photoactivatable substrates: a material-based approach for dissecting cell migration", J. Nakanishi, *Chem. Rec.* in press (Review paper).

16 Nano- and microstructured biomaterials for regenerative medicine

G. Chen, N. Kawazoe

Nano- and microstructured biomaterials play an important role in regenerative medicine to control stem cell functions and to guide the regeneration of new tissues and organs. We developed a few types of highly functional biomaterials that mimic the nanostructured microenvironments surrounding cells *in vivo*. The biomaterials showed specific control of cell functions such as adhesion, spreading, proliferation, and differentiation and promoted tissue regeneration.

By combining cells, biomaterial scaffolds, and bioactive molecules, tissue regeneration has been shown to be a promising therapeutic approach in treating disease and injury. Biomaterial scaffolds provide physiochemical and biological cues to control cell functions for tissue regeneration. Ideally, biomaterial scaffolds should provide the same nano- and microenvironments for seeded cells as those of extracellular matrices (ECMs) existing *in vivo*.

Stepwise tissue development matrices that mimic the *in vivo* nanostructured developmental ECMs were prepared by decellularizing serially differentiated mesenchymal stem cells (MSCs). Stepwise osteogenesis- and adipogenesis-mimicking matrices that mimicked the ECMs throughout each step of osteogenesis and adipogenesis of MSCs were prepared by controlling the osteogenic and adipogenic differentiation of MSCs[1). Furthermore, biomimetic porous scaffolds were prepared by 3D culture of cells in a selectively removable poly (lactide-co-glycolide) template. Autologous ECM scaffolds prepared by this method showed minimized host tissue responses during implantation. These biomimetic nanostructured matrices and scaffolds are useful for tissue regeneration and basic biological research.

A novel method using preprepared ice particulates as living porogen materials was developed to control precisely the pore structures of biomaterial scaffolds. The method was used to prepare spatially micropatterned pore structures and to micropattern bioactive molecules in the porous scaffolds[2)]. The micropatterned porous scaffolds were used for regeneration of cartilage, skin, capillary, and muscle tissues. To study the effects of biological and physiochemical cues on stem cell functions, photoreactive poly (vinyl alcohol) was synthesized and used to prepare various types of micropatterns. The micropatterns were designed to control cell size, shape, and aspect ratio to investigate their effects on stem cell functions[3)]. Stemness, nanomechanical properties, cell/nanomaterial interactions, and cell differentiation were investigated using the ingeniously designed micropatterns. The micropatterned cells showed different behaviors, indicating that the cell morphogenesis regulated by micropatterns played critical roles in stem cell fate determination.

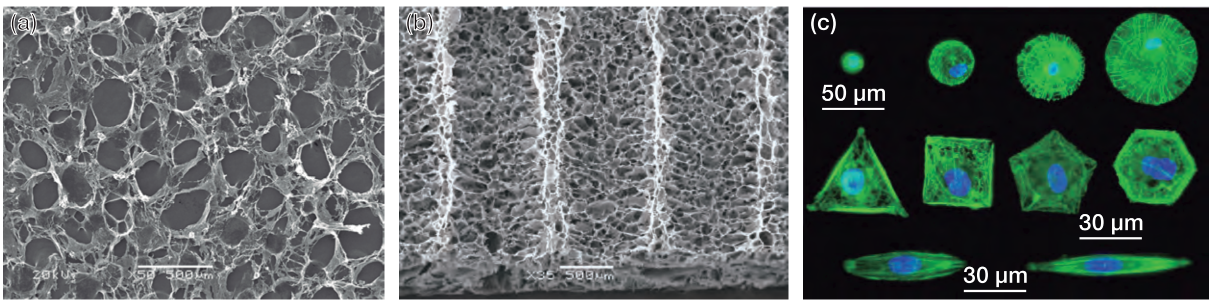

Fig. 1 **(a)**Biomimetic ECM scaffold prepared from cultured cells. **(b)** Micropatterned scaffold prepared using the ice particulate method. **(c)** Stem cell morphology controlled by micropatterns with various geometry.

Main Papers

1) "Development of extracellular matrices mimicking stepwise adipogenesis of mesenchymal stem cells", T. Hoshiba, N. Kawazoe, T. Tateishi, G. Chen, *Adv. Mater.* **22** (2010) 3042.
2) "Preparation of collagen porous scaffolds with micropatterned structures", H.H. Oh, Y.G. Ko, H. Lu, N. Kawazoe, G. Chen, *Adv. Mater.* **24** (2012) 4311.
3) "Manipulating cell nanomechanics using micropatterned surfaces", X. Wang, X. Hu, N. Kawazoe, Y. Yang, G. Chen, *Adv. Funct. Mater.* **26** (2016) 7634.

17 Silicon nanocrystals for bioimaging in the near-infrared biological optical window

F. M. Winnik Co-workers: C. Sourov, G. Beaune, N. Shirahata

Functional water-dispersible near-infrared (NIR)-emitting nanoparticles (NPs) adapted for two-photon excitation cellular imaging were developed starting from octadecyl-terminated silicon nanocrystals (ncSi-OD) with narrow photoluminescence (PL) spectra free of emission tails and continuously tunable over the NIR biological window. Their PL quantum yields (QYs) exceed 30% and their PL lifetimes are 300 µsec or longer. The NPs, which are very low in toxicity, were internalized in cells and imaged *in vitro*.

We have reported new ncSi-OD based biomarkers adapted for two-photon fluorescence cellular imaging in the NIR range[1]. As shown schematically in Fig. 1(a), the water-borne NPs consist of a core-double-shell structure where the core consists of individual ncSi covalently bound to hydrocarbon chains (ncSi-OD), ensuring high PL QYs, coated with an amphiphilic shell made of a Food and Drug Administration-approved amphiphilic polymer (Pluronic F127) that provides water dispersibility. The NPs retained their colloidal stability and emission characteristics (Fig. 1(b)) for extended periods under physiological conditions (pH 7.4, 0.1 M NaCl) in the presence of serum albumin, the major blood protein. *In vitro* two-photon fluorescence imaging with NIR excitation confirmed that the double-shelled NPs were internalized by NIH3T3 cells and did not penetrate the cell nucleus (Fig. 1(c)). HiLyte Fluor 750 amine was linked via an amide linkage to SiNPs prepared with Pluronic F127-COOH, as the first demonstration of functional NIR-emitting water-dispersible ncSi-based NPs, opening up many interesting possibilities in bioimaging and theragnostics in the near future.

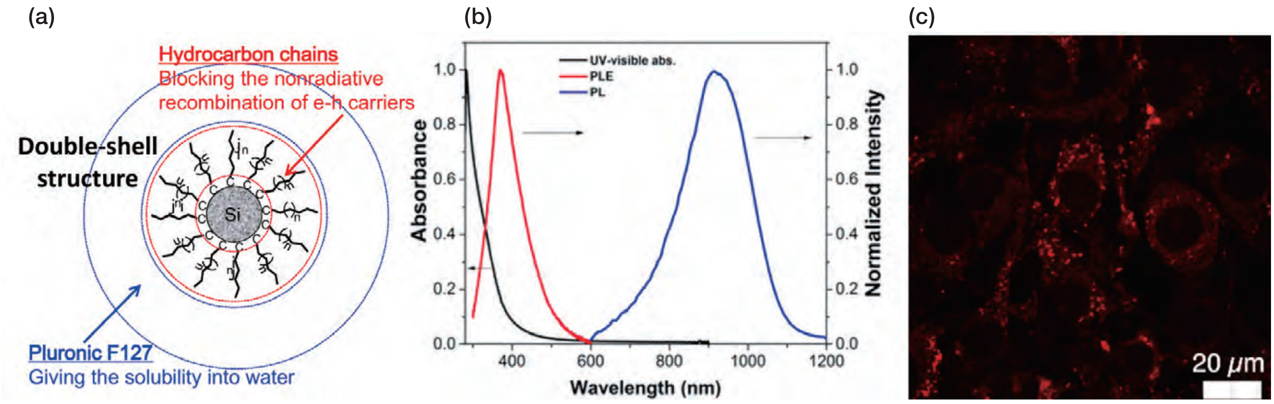

Fig. 1 **(a)**Double-shelled structure of water-borne ncSi-based NPs. **(b)** Typical ultraviolet-visible spectroscopy, PL excitation, and PL spectra of the water-borne Si-based NPs before size separation. **(c)** Micrograph of NIH3T3 cells observed with confocal fluorescence microscopy.

Main Papers

1) "Functional double-shelled silicon nanocrystals for two-photon fluorescence cell imaging: spectral evolution and tuning", S. Chandra, B. Ghosh, G. Beaune, U. Nagarajan, T. Yasui, J. Nakamura, T. Tsuruoka, Y. Baba, N. Shirahata, F.M. Winnik, *Nanoscale* **8** (2016) 9009.

2) "One-pot synthesis of water soluble highly fluorescent silica nanoparticles," S. Chandra, G. Beaune, N. Shirahata, F.M. Winnik, *J. Mater. Chem. B* (2016), accepted for publication.

18 Artificial photosynthesis: nature-inspired nanoarchitectonics for efficient solar–chemical conversion

J. Ye Co-workers: Z. Yi, H. Zhou

We have been challenging artificial photosynthesis, which offers potential solutions for global warming and energy shortage issues. The new material Ag_3PO_4 with the world's highest quantum efficiency (approaching that of natural photosynthesis) in photocatalytic water oxidation was developed under unique material-designing guidelines. Sophisticated control of the surface/interface structure to mimic the structural and functional elements in nature enables efficient light harvesting, charge separation, and gas diffusion/conversion, making a big step toward achieving high-efficiency artificial photosynthesis.

As nano-life science-inspired nanoarchitectonics, we developed a unique strategy for constructing a promising 3D artificial photosynthetic system (APS) for efficient CO_2 photoreduction into hydrocarbon fuels. Natural leaves are a synergy of complex architectures and functional components to produce amazing biomachinery for photosynthesis. Using cherry tree leaves as the template, we successfully fabricated perovskite titanates (e.g., $SrTiO_3$, $CaTiO_3$) with a modified sol-gel method. After acid treatment and calcination at 600°C, the organics could be removed completely, leaving crystalline perovskite titanates. The material obtained preserves the morphological features of leaves at multiscaled levels. The leaf-architectured $SrTiO_3$ exhibits about a 3.5–4-fold improvement in activities compared with reference $SrTiO_3$ synthesized without templates. A further mechanism study revealed that the enhanced conversion efficiency of CO_2 into hydrocarbon fuels can be attributed to the synergistic effects of the efficient mass flow/light-harvesting network relying on the morphological replacement of a conceptual prototype leaf 3D architecture.

We also successfully developed a prototype basic artificial photosynthetic unit by mimicking the nanoscale-level structure of natural photosynthesis, which occurs in nanolayered thylakoid stacks (granum) where photosynthetic pigments, functional proteins, electron carriers, and co-factors are precisely arranged (Fig. 1(b,c)). By interfacing a triple junction, with polymeric g-C_3N_4 as an active water-splitting and CO_2 reduction photocatalyst, Au nanoparticles as a co-catalyst, and zeolitic imidazolate frameworks (ZIF-9) as an electron mediator as well as CO_2 activator, we efficiently converted solar energy into hydrocarbon fuels and hydrogen. We found that the linkage between ZIF-9 and g-C_3N_4 through π-π interaction is essential for enhancing activity. The artificial unit provides an important biomimetic step down a path aligned with low-cost APS manufacturing that is required for inexpensive solar-to-fuel systems.

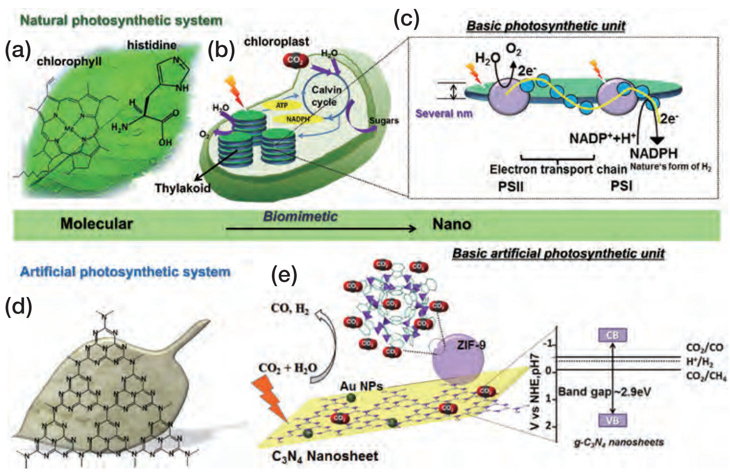

Fig. 1 Schematic illustration and comparison of natural and artificial photosynthetic systems. **(a)** Natural leaf with abundant nonmetallic elements at the fundamental (molecular) level. **(b)** Simplified scheme of light-driven reactions of photosynthesis in a chloroplast. **(c)** Basic photosynthetic unit. **(d)** Molecular structure of polymeric g-C_3N_4. **(e)** Artificial photosynthesis on the basic artificial photosynthetic unit.

Main Papers

1) "An orthophosphate semiconductor with photooxidation properties under visible-light irradiation", Z. Yi, J. Ye, N. Kikugawa, T. Kako, S. Ouyang, H. Stuart-Williams, H. Yang, J. Cao, W. Luo, Z. Li, Y. Liu, R.L. Withers, *Nature Mater.* **9** (2010) 559.

2) "Leaf-architectured 3D hierarchical artificial photosynthetic system of perovskite titanates towards CO_2 photoreduction into hydrocarbon fuels", H. Zhou, J. Guo, P. Li, T. Fan, D. Zhang, J. Ye, *Sci. Rep.* **3** (2013) 1667.

3) "Biomimetic polymeric semiconductor based hybrid nanosystems for artificial photosynthesis towards solar fuels generation via CO_2 reduction", H. Zhou, P. Li, J. Liu, Z. Chen, L. Liu, D. Dontsova, R. Yan, T. Fan, D. Zhang, J. Ye, *Nano Energy* **25** (2016) 128.

19 Novel thermoelectric materials: steps toward the first wide-scale power generation from waste heat

T. Mori, N. Tsujii, I. Ohkubo Co-worker: A. U. Khan

We achieved a >100% increase in the thermoelectric figure of merit ZT in the champion skutterudite material by utilizing phase diagrams to create surprisingly controlled, effective porosity in a material. As a novel principle, we also discovered thermoelectric enhancement in magnetic semiconductors like chalcopyrite. Novel nitrides are also proposed as a thermoelectrically superior new group of materials to extensively studied oxides, while novel borides were developed with excellent p, n control.

Over half of all fossil fuels consumed is lost in the form of waste heat. Thermoelectrics represent conversion of part of this huge amount of energy in the form of useful solid-state conversion, but are still not widely applied because of insufficient material performance and various material and other factors. We reported several striking results that are breakthroughs in resolving some critical issues.

Novel nanostructuring is achieved by utilizing phase diagrams to create surprisingly controlled, effective porosity in a material, leading to effective phonon-selective scattering and a >100% increase in the thermoelectric figure of merit ZT in the champion skutterudite material. High ZT is achieved without rare earth and without depending on conventional rattling phenomena, thereby keeping material costs and risks low, and improving oxidation resistance beneficial to scaling up production.

We discovered enhanced thermoelectric properties in magnetic semiconductors like chalcopyrite. Electron–magnon interaction and large effective masses are indicated to enhance the Seebeck coefficient. A 40-fold enhancement of ZT was also observed in a boride, which appeared to result from the mixed valency of samarium. We propose that magnetism can be a new effective tuning mechanism for thermoelectrics, superior to conventional band engineering that is difficult in actual application.

Novel nitrides isoelectronic to well-studied thermoelectric oxides were also investigated and superior properties and interesting anisotropy were revealed, yielding a promising group of new materials. Novel borides like ytrrium aluminoboride and Zr-doped beta-boron were also developed with excellent p, n control characteristics and are being considered for high-temperature topping cycles to enhance the output of power plants.

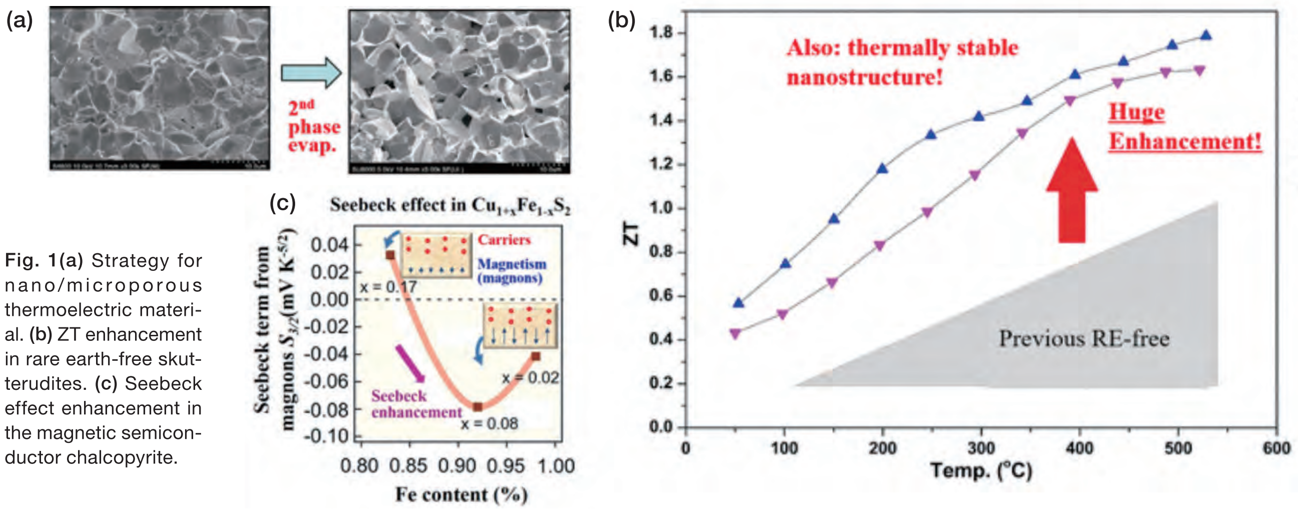

Fig. 1(a) Strategy for nano/microporous thermoelectric material. (b) ZT enhancement in rare earth-free skutterudites. (c) Seebeck effect enhancement in the magnetic semiconductor chalcopyrite.

Main Papers

1) "Nano-micro-porous skutterudites with 100% enhancement in ZT for high performance thermoelectricity", A.U. Khan, K. Kobayashi, D. Tang, Y. Yamauchi, K. Hasegawa, M. Mitome, Y. Xue, B. Jiang, K. Tsuchiya, D. Golberg, Y. Bando, T. Mori, *Nano Energy* **31** (2017) 152.
2) "Thermoelectricity generation and electron-magnon scattering in natural chalcopyrite mineral from deep-sea hydrothermal vents", R. Ang, A.U. Khan, N. Tsujii, K. Takai, R. Nakamura, T. Mori, *Angew. Chem. Int. Edit.* **54** (2015) 12909.
3) "Two-dimensional layered complex nitrides AMN_2 as a new class of thermoelectric materials", I. Ohkubo, T. Mori, *Chem. Mater.* **26** (2014) 2532.

20 Piezotronics and piezophototronics: novel nanomaterials and nanodevices

Z. L. Wang Co-workers: **K. C. Pradel, Y. Ding, X. Wen, W. Wu, F. Zhang**

We pioneered in exploring the effect of piezopotential on the transport behavior of charge carriers in electronic and optoelectronic nanodevices. The new fields of piezotronics and piezophototronics were created by utilizing piezopotential inside material crystals as a "gate" potential to control charge carrier transport behavior for electronics and optoelectronics. For that purpose, we developed several novel materials/structures such as p-type ZnO nanowires, ZnO p–n homojunctions, and heterojunctions. The research results indicate potential applications in strain/force-triggered electronic devices, sensors, and logic units.

Piezoelectricity is the effect of electrical potential build-up inside material under strain. It has been known for centuries, with numerous piezoelectric materials discovered. Natural materials with the largest piezoelectric coefficients usually have perovskite structures, such as $Pb(Zr, Ti)O_3$, which have been widely utilized in electromechanical sensors, actuators, and energy harvesters. However, since these materials are usually insulators, they are not very useful when coupled with electronic devices. Wurtzite piezoelectric materials, including ZnO, GaN, InN, and CdS, are semiconducting materials that have been intensively studied in electronics and optoelectronics. Our study of piezotronics and piezophototronics involves coupling the piezoelectric property of wurtzite materials to the study of electronics and optoelectronics to enable the control of carrier transport through strains/forces. A full understanding of the theory of piezotronics to enable novel applications requires investigation of the feasibility of novel materials/structures, for example, p-type piezoelectric semiconductors, n–p homojunctions, etc.

For ZnO nanomaterials, we first successfully demonstrated the growth of ultralong p-type ZnO nanowires up to 60 µm in length using a low-temperature solution growth method (Fig. 1(a and b))[1]. After verifying the carrier type using well-established experimental methods, we performed the first reported investigation of the piezotronic effect in p-type ZnO (Fig. 1(c)) and further demonstrated the sensing and energy harvesting applications of p-type piezotronic devices. Furthermore, we first demonstrated ZnO n–p homojunction nanostructures[2] with outstanding performance. That research provided material structures that will enable the function of strain/force-gated electronics through piezotronic effects.

For heterostructures, we demonstrated the potential for enhancing the performance of photodetectors, solar cells, etc., through piezophototronic effects. For example, we fabricated a novel microwire-photodetector with a branched ZnO-CdS double-shell NW array grown on the surface of a carbon fiber, with greatly enhanced responsivity[3].

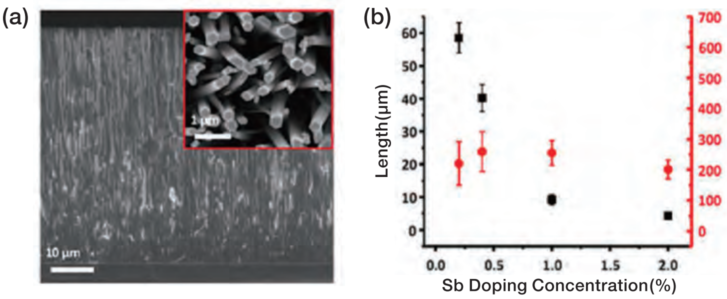

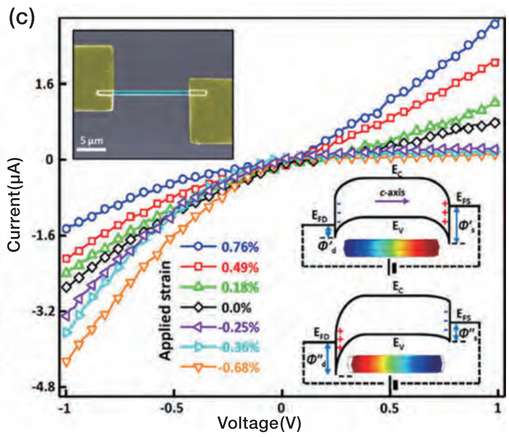

Fig. 1(a) p-Type ZnO nanowires grown; **(b)** growth length and diameter of a ZnO nanowire versus the Sb doping concentration; **(c)** ID-VDS of the fabricated ZnO nanowire field-effect transistor under different applied strains. The inset in the upper-left corner shows a scanning electron microscopic image of the device, with colors added. The inset in the lower-right corner shows the mechanism of piezotronics.

Main Papers

1) "Piezotronic effect in solution-grown p-type ZnO nanowires and films", K.C. Pradel, W. Wu, Y. Zhou, X. Wen, Y. Ding, Z.L. Wang, *Nano Lett.* **13** (2013) 2647.
2) "Solution-derived ZnO homojunction nanowire films on wearable substrates for energy conversion and self-powered gesture recognition", K.C. Pradel, W. Wu, Y. Ding, Z.L. Wang, *Nano Lett.* **14** (2014) 6897.
3) "Pizeo-phototronic effect enhanced visible/UV photodetector of a carbon-fiber/ZnO-CdS double-shell microwire", F. Zhang, S. Niu, W. Guo, G. Zhu, Y. Liu, X. Zhang, Z.L. Wang, *ACS Nano* **7** (2013) 4537.

21 Interface science of batteries, solar cells, and catalysts via supercomputer simulations

Y. Tateyama Co-worker: K. Sodeyama

Atomic and electronic processes at buried interfaces are still open questions because of the difficulties in *in-situ* experimental observations as well as accurate calculations. We developed highly efficient first-principles sampling codes for large-scale supercomputers like the K computer and revealed the microscopic mechanisms of those interfacial issues such as redox processes, electric double-layers, and water dissociation in energy and environmental materials.

For next-generation batteries, solar cells, and catalysts, understanding and designing the (solid–liquid and solid–solid) interfaces are indispensable. However, atomic and electronic processes at buried interfaces are still open questions because of the difficulties in *in-situ* experimental observations as well as accurate calculations. We developed highly efficient first-principles sampling codes based on density functional theory for large-scale supercomputers like the K computer, a flagship supercomputer in Japan, and addressed the crucial issues in batteries, solar cells, and catalysts, in collaboration with leading experimentalists and industries.

Concerning battery issues, we demonstrated a new mechanism of the reductive decomposition of typical organic electrolytes and a novel mechanism called "near-shore aggregation" for the subsequent formation of solid electrolyte interphase (SEI) film on the electrode interface. We also clarified the origins of improved redox stability and fast ion transport in superconcentrated electrolytes, which have attracted considerable interest recently. Probable interfacial structures and the expected functions for dye-sensitized solar cells and perovskite solar cells were also demonstrated. Moreover, we revealed the interfacial redox reactivity depending on the surface terminations of diamond electrodes and enhanced water dissociation on CeO_2/H_2O interfaces with a Pt nanoparticle. These findings on complicated rare events allow the establishment of a new field, microscopic interface science. Besides, our computational researches will play crucial roles in the transformation of energy management in modern society.

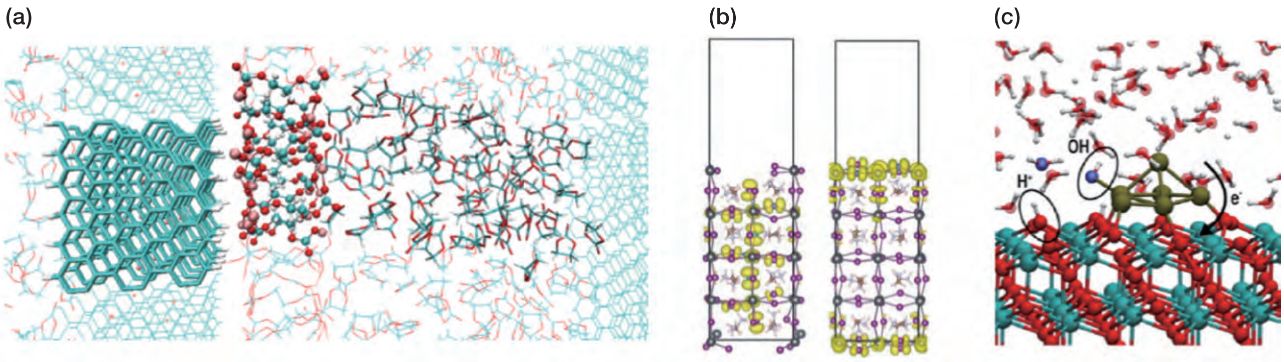

Fig. 1 **(a)** Calculated probable SEI film model in a Li-ion battery. **(b)** Calculated interface models of $CH_3NH_3PbI_3$ in perovskite solar cells. **(c)** Water dissociation process on CeO_2/Pt nanoparticle/H_2O interfaces.

Main Papers

1) "Additive effect on reductive decomposition and binding of carbonate-based solvent toward solid electrolyte interphase formation in lithium-ion battery," K. Ushirogata, K. Sodeyama, Y. Okuno, Y. Tateyama, *J. Am. Chem. Soc.* **135** (2013) 11967.
2) "Sacrificial anion reduction mechanism for electrochemical stability improvement in highly concentrated Li-salt electrolyte," K. Sodeyama, Y. Yamada, K. Aikawa, A. Yamada, Y. Tateyama, *J. Phys. Chem. C* **118** (2014) 14091.
3) "Termination dependence of tetragonal $CH_3NH_3PbI_3$ surfaces for perovskite solar cells," J. Haruyama, K. Sodeyama, L. Han, Y. Tateyama, *J. Phys. Chem. Lett.* **5** (2014) 2903.
4) "Catalytic proton dynamics at the water/solid interface of ceria supported Pt clusters," M.F. Camellone, F.N. Ribeiro, L. Szabova, Y. Tateyama, S. Fabris, *J. Am Chem. Soc.* **138** (2016) 11560.

22 Large-scale first-principles calculations and experiments for the design of nanoscale devices

T. Miyazaki, D. R. Bowler, N. Fukata

To enable first-principles electronic structure calculations using density functional theory (DFT) to be performed on systems that correspond to practical nanoscale devices and materials, we developed a world-leading linear-scaling DFT code: CONQUEST. Using CONQUEST, we conducted collaborative theory-experimental research on Si/Ge core-shell nanowires.

The control and growth of semiconductor microstructures and nanostructures have driven the modern electronics industry. As device sizes shrink, an atomistic description of the structure of surfaces and interfaces in semiconductor nanostructures is becoming increasingly valuable.

First-principles calculations based on DFT are a powerful tool that can provide reliable information on the atomic positions and electronic structures of materials independently from experiments. However, since the cost of DFT calculations is expensive and increases rapidly with the cube of the number of atoms N, it is almost impossible to treat systems containing more than a few thousand atoms using standard DFT implementations. Thus, it was very difficult to model practical nanoscale devices by DFT methods. To overcome this problem, we developed a linear-scaling DFT code, CONQUEST, for which the computational cost is only proportional to N. With CONQUEST, we can perform robust, accurate electronic structure calculations, including structural relaxations and molecular dynamics, on very large systems containing more than one million atoms.

Using CONQUEST, we performed DFT studies of three-dimensional Ge nanoislands on Si(001) substrates and Ge/Si core-shell nanowires (Fig. 1(a)). For the nanowires, which are a promising material for next-generation vertical transistors, we performed collaborative theory-experimental research. Experimentally, we can control the radius of the core and thickness of the shell of the nanowires with high crystallinity. Properties of the core-shell nanowires are expected to depend strongly on the size, interface between Si and Ge, impurity distribution, and other structural factors, which could not be modeled before. Using CONQUEST, we succeeded in calculating the strain distribution in the nanowires and electronic structure near the Fermi level (Fig. 1(b)). Based on those calculated results, we synthesized Ge/Si core-shell nanowires and found conclusive evidence of hole gas accumulation in the core-shell nanowires experimentally.

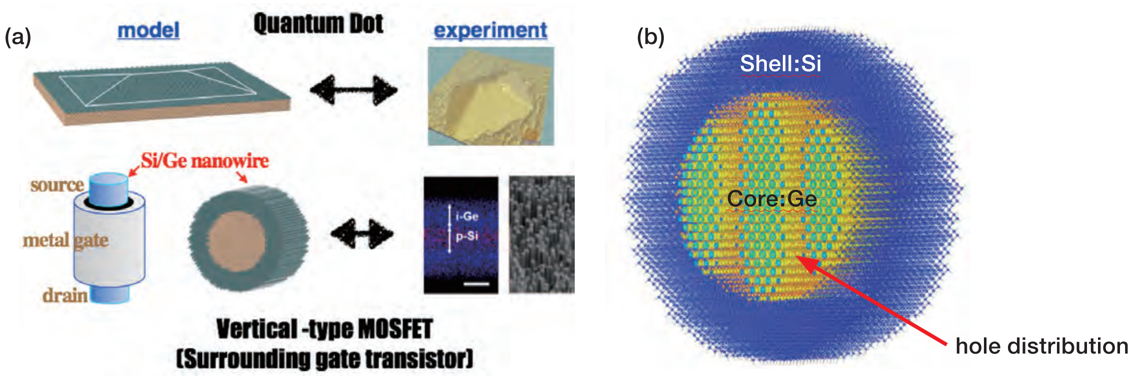

Fig. 1(a) (upper) Optimized structure of a Ge nanoisland on Si(001) substrate calculated using CONQUEST and experimental structure. (lower) Atomic models of Si/Ge core-shell nanowire, along with transmission electron microscopic and scanning electron microscopic measurements and schematic representation of how nanowires can be used in transistors. **(b)** Example of the distribution of a hole carrier in a Ge/Si core-shell nanowire.

Main Papers

1) "O(N) methods in electronic structure calculations", D.R. Bowler, T. Miyazaki, *Rep. Prog. Phys.* **75** (2012) 036503.
2) "Stable and Efficient Linear Scaling First-Principles Molecular Dynamics for 10000+ Atoms," M. Arita, D.R. Bowler, T. Miyazaki, *J. Chem. Theory Comput.* **10** (2014) 5419.
3) "Clear Experimental Demonstration of Hole Gas Accumulation in Ge/Si Core-Shell Nanowires", N. Fukata, M. Yu, W. Jevasuwan, T. Takei, Y. Bando, W. Wu, Z.L. Wan, *ACS Nano* **9** (2015) 12182.

23 Surface atomic-layer superconductors on silicon: macroscopic supercurrents and Josephson vortices

T. Uchihashi, X. Hu Co-workers: S. Yoshizawa, T. Kawakami

We demonstrated that surface atomic layers on silicon can become superconducting by directly observing robust macroscopic supercurrents for the first time. In addition, our scanning tunneling microscope (STM) observations and theoretical calculations revealed the presence of Josephson vortices at atomic steps. These findings open a route for creating superconducting devices with Josephson junctions based on surface atomic-layer materials on silicon.

Atomic-layer 2D materials such as graphene have attracted extensive attention because of their novel properties and wide range of applications. We demonstrated for the first time that atomic-layer 2D materials can become superconducting by directly observing macroscopic supercurrents. Fig. 1(a) shows an STM image of an indium atomic layer grown on a silicon surface and the temperature dependence of its electrical resistance. The data show a sharp superconducting transition at 2.8 K. We also found that the critical supercurrent density is as large as 6×10^5 A/cm^2 at 1.8 K, which is comparable to typical values of practical superconducting materials. It is surprising that atomically thin superconductors retain such robustness.

One of the unique features of surface atomic-layer materials is the presence of atomic steps. Since the superconducting regions of flat terraces can be weakly coupled there, atomic steps can work as Josephson junctions (for schematic illustration, see Fig. 1 (b)). While this idea was indicated by the temperature dependence of critical supercurrent density, more direct evidence was given by observation of Josephson vortices. Fig. 1(c) shows an STM image of superconducting vortices trapped at atomic steps. The vortices appear elongated along the steps and the image contrasts of the core regions are suppressed, indicating that superconductivity recovers significantly within the usually normal-like cores. The fact that these vortices are actually Josephson vortices was firmly established with the help of microscopic theoretical calculations. Our findings show that a high density of supercurrent can run over a macroscopically large distance despite the presence of atomic steps and that atomic steps play the role of Josephson junctions. Therefore, surface atomic-layer superconductors on silicon can be potentially used for superconducting devices with atomic-scale thickness.

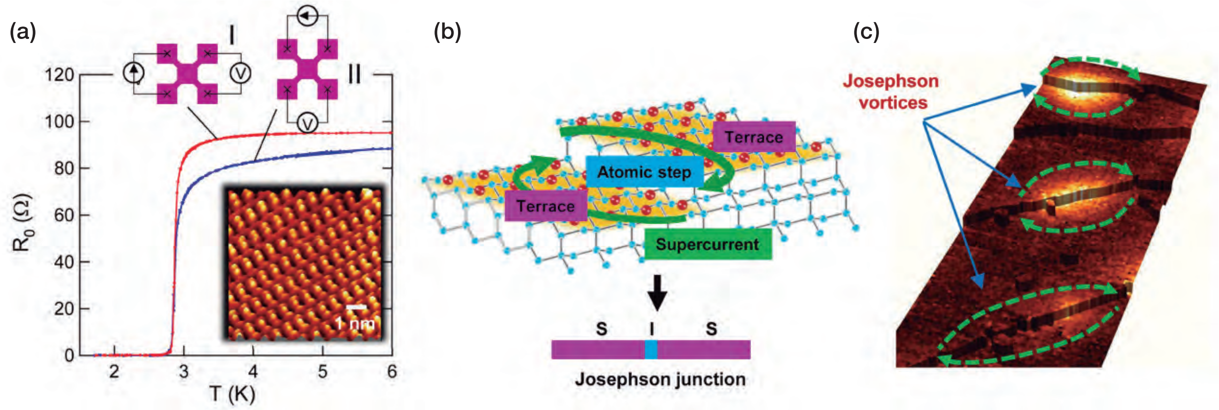

Fig. 1 Superconducting transition and Josephson vortices of surface atomic layers on silicon. **(a)** Superconducting transition revealed by electron transport measurement and STM image of an indium atomic layer on silicon. **(b)** Schematic illustration of a Josephson vortex at an atomic step. **(c)** STM image of Josephson vortices.

Main Papers

1) "Macroscopic superconducting current through a silicon surface reconstruction with indium adatoms: Si(111)-($\sqrt{7}\times\sqrt{3}$)-In", T. Uchihashi, P. Mishra, M. Aono, T. Nakayama, Phys. Rev. Lett. **107** (2011) 207001 (highlighted as an Editor's Suggestion and a Viewpoint in *Physics*).
2) "Resistive phase transition of the superconducting Si(111)-($\sqrt{7}\times\sqrt{3}$)-In surface", T. Uchihashi, P. Mishra, T. Nakayama, Nanoscale Res. Lett. **8** (2013) 167.
3) "Imaging Josephson vortices on the surface superconductor Si(111)-($\sqrt{7}\times\sqrt{3}$)-In using a scanning tunneling microscope", S. Yoshizawa, H. Kim, T. Kawakami, Y. Nagai, T. Nakayama, X. Hu, Y. Hasegawa, T. Uchihashi, Phys. Rev. Lett. **113** (2014) 247004 (highlighted as an Editor's Suggestion and a Synopsis in *Physics*).

24 Development of novel electrocatalysts for highly efficient energy conversion reactions: theoretical prediction and experimental proof

K. Uosaki, H. Noguchi Co-workers: G. Elumalai, H. C. Dinh

Boron nitride (BN), an insulator with a wide band gap, supported on Au (BN/Au) is predicted theoretically and proved experimentally to act as an electrocatalyst for oxygen reduction reaction. Although BN/Au reduces oxygen to H_2O_2 by a 2-electron process, oxygen can be reduced to H_2O by a 4-electron process by decorating BN with Au nanoparticles. BN/Au also works as a hydrogen evolution reaction catalyst with efficiency close to that of Pt. Theoretical study shows that some edge atoms provide energetically favored sites for intermediate adsorption.

Hydrogen plays a key role in a sustainable society based on renewable energy, and the development of efficient electrochemical energy conversion processes, e.g., water electrolysis to produce hydrogen and fuel cells to covert hydrogen and oxygen to electricity and water, is required. We developed a novel electrocatalytic system for oxygen reduction reaction (ORR) and hydrogen evolution reaction (HER) based on hexagonal boron nitride (h-BN), an insulator with a wide band gap.

Theory predicts that the band gap of h-BN can be considerably reduced if defects are introduced and/or it is placed on metal substrates and that reduction of O_2 to H_2O_2 is possible at BN on an electrocatalytically inert Au electrode[1]. It is proved experimentally that Au electrodes modified with various types of h-BN, BN nanotubes, BN nanosheets (BNNS), and RF-sputtered BN, act as effective ORR electrocatalysts[1,2]. Overpotential for ORR at a Au electrode is reduced by 0.27 V by BNNS modification and oxygen is mainly reduced to H_2O_2 via the 2-electron process (Fig. 1(a)). As theory suggests that the BN/Au edge provides favored sites for oxygen adsorption, decorating BNNS with Au nanoparticles and using smaller BNNS not only reduce overpotential but also make 4-electron reduction to H_2O possible.

Considering the high hydrogen adsorption/storage ability of BN, electrocatalytic activity for HER is examined. Overpotential at the Au electrode is reduced significantly by BN modification (Fig. 1(b)). The smaller the BNNS size, the higher the HER efficiency. The overpotential at BNNS (0.1–0.22 μm)/Au is only 30 mV larger than that at a Pt electrode. Theoretical calculation shows that the origin of small overpotential is due to the energetically favored edge sites for intermediate state of HER, i.e., adsorbed hydrogen[3].

The present combined theoretical and experimental study opens a new route to develop novel electrocatalysts.

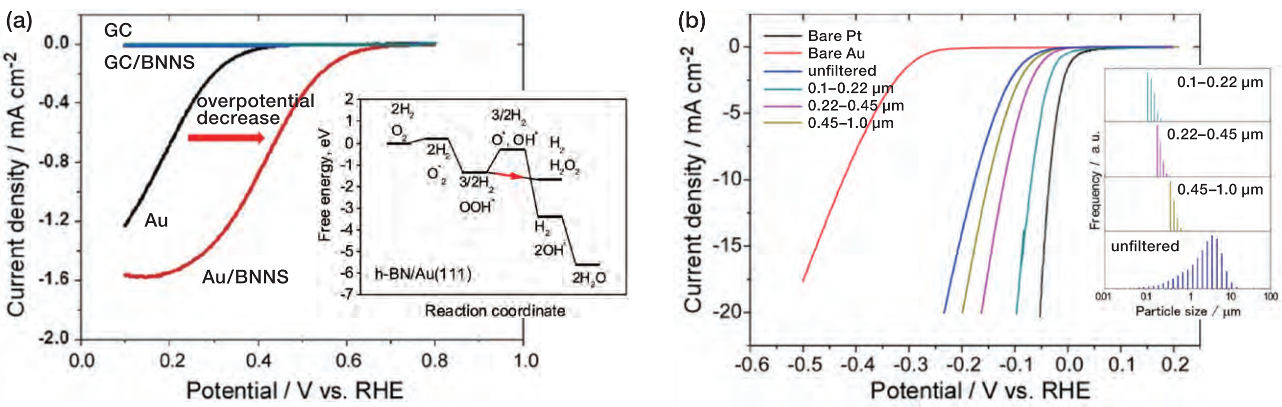

Fig. 1(a) ORR current at bare Au, BNNS-modified Au, GC, and BNNS-modified glassy carbon (GC) in O_2-saturated 0.5 M H_2SO_4 solution. Scan rate: 10 mV/s. Inset: Free energy diagram ORR. **(b)** HER current at bare Pt, bare Au, BNNS (unfiltered)/Au, BNNS (0.45–1.0 μm)/Au, BNNS (0.22–0.45 μm)/Au, BNNS (0.1–0.22 μm)/Au in Ar-saturated 0.5 M H_2SO_4 solution. Scan rate: 1 mV/s. Inset: Size distribution of unfiltered 0.45–1.0 μm, 0.22–0.45 μm, 0.1–0.22 μm BNNS.

Main Papers

1) "Boron nitride nanosheet on gold as an electrocatalyst for oxygen reduction reaction: Theoretical suggestion and experimental proof", K. Uosaki, G. Elumalai, H. Noguchi, T. Masuda, A. Lyalin, A. Nakayama, T. Taketsugu, *J. Am. Chem. Soc.* **136** (2014) 6542.
2) "Electrocatalytic activity of various types of h-BN for the oxygen reduction reaction", G. Elumalai, H. Noguchi, K. Uosaki, *Phys. Chem. Chem. Phys.* **16** (2014) 13755.
3) "Highly efficient electrochemical hydrogen evolution reaction at insulating boron nitride nanosheet on inert gold substrate", K. Uosaki, G. Elumalai, H.C. Dinh, A. Lyalin, T. Taketsugu, H. Noguchi, *Sci. Rep.* **6** (2016) 32217.

III

Other Remarkable Research Results

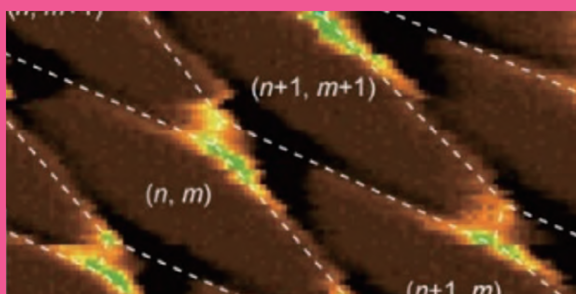

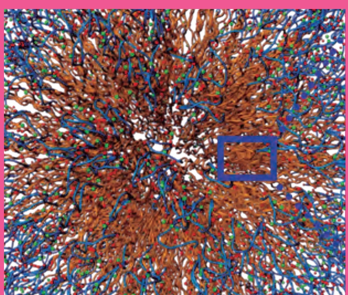

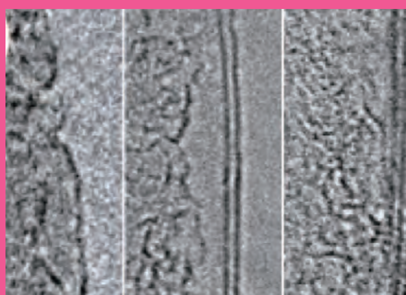

25 Boron nitride nanostructured materials: novel synthesis by "chemical blowing" and applications

Y. Bando, D. Golberg

The mass production of boron nitride (BN) low-dimensional materials at gram levels was successfully achieved via synthetic routes of "chemical blowing" and carbothermal reduction. Such abundant BN nanotube and nanosheet products were applied to advanced composite materials as fillers, especially for fabricating polymeric packaging materials with greatly enhanced thermal conductivity allowing for quick release of heat in diverse electronic devices.

BN, a structural counterpart of graphite with sp^2-hybrid layers, features excellent electrical insulation, wide bandgap, superb thermal and chemical stability, and high thermal conductivity. It has many complementary applications to its carbon analog, e.g., electrically insulating thermally conductive fillers in composite materials for thermal management. However, the production of BN nanomaterials is still insufficient, which largely limits their study and full realization of application potentials. We have recently successfully synthesized BN nanotubes and nanosheets on a large scale.

We developed an effective production method for gram-level, high-quality BN nanotubes through chemical vapor deposition of boron and metal oxide precursors. We also synthesized large quantities of BN nanosheets by a chemical blowing method[1,2] and fabricated single-crystalline nanosheets using a biomass-directed carbothermal reduction yielding 20 g of product per run (Fig. 1(a)). The BN nanosheets have an average lateral size of ~20 μm and the thickness of ~5 nm (Fig. 1(b,c)), making them especially suitable for forming composites. The BN nanotubes and nanosheets were filled into a polymeric matrix, and such composite materials had a 20-fold increase in thermal conductivity compared with blank polymers (Fig. 1(d))[3]. This achievement is very useful for heat-release insulating packaging in down-sized high-speed electronic devices. The BN nanomaterials were also used for fabricating light but strong composites, e.g., reinforced aluminum matrices. Moreover, the synthesis methods were extended to produce other nanosheet materials, e.g., strutted graphenes[2].

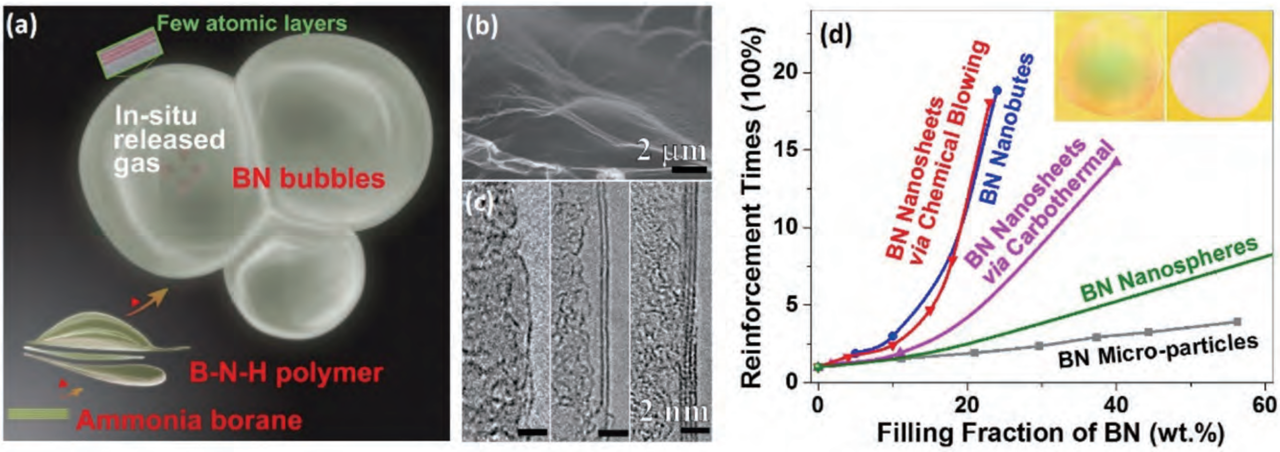

Fig. 1 (a) Chemical blowing process for synthesizing BN nanosheets. (b) Scanning electron microscope image of a BN nanosheet. (c) High-resolution transmission electron microscope images of BN nanosheets with 1–3 atomic layers. (d) Thermal conductivity increase in BN-filled polymeric composites. The insets show photos of a blank epoxy and that with a 40 wt.% BN-nanosheet loading fraction.

Main Papers

1) "Chemical blowing of thin-walled bubbles: High-throughput fabrication of large-area, few-layered BN and Cx-BN nanosheets," X.B. Wang, C. Zhi, L. Li, H. Zeng, C. Li, M. Mitome, D. Golberg, Y. Bando, *Adv. Mater.* **23** (2011) 4072.
2) "Three-dimensional strutted graphene grown by substrate-free sugar blowing for high-power-density supercapacitors," X.B. Wang, Y. Zhang, C. Zhi, X. Wang, D. Tang, Y. Xu, Q. Weng, X. Jiang, M. Mitome, D. Golberg, Y. Bando, *Nat. Commun.* **4** (2013) 2905.
3) "Biomass-directed synthesis of 20 g high-quality boron nitride nanosheets for thermoconductive polymeric composites," X.B. Wang, Q. Weng, X. Wang, X. Li, J. Zhang, F. Liu, X. Jiang, H. Guo, N. Xu, D. Golberg, Y. Bando, *ACS Nano* **8** (2014) 9081.

26 Nanoarchitectured porous materials with metallic walls

Y. Yamauchi

Nanoporous architectures with metallic walls are necessary for higher catalytic performance. A new "micelle-assembly" approach for the synthesis of mesoporous metals with a narrow pore-size distribution enables the synthesis of more complex mesoporous architectures with multifunctional properties, which cannot be achieved by conventional methods (i.e., hard- and soft-templating approaches).

Recent research activities are rapidly being extended to various nonsiliceous mesoporous materials with different framework compositions, such as carbons, metals, metal oxides, sulphides, inorganic–organic hybrid materials, and polymers. Even though there have been many reports on the successful preparation of nonsiliceous mesoporous materials, maintaining the stable integrity of structures is still a challenging issue because mesopores tend to collapse during the crystallization of pore walls and/or the template removal process. Among these materials, mesoporous metals have attracted a great deal of attention. Owing to their fascinating physicochemical properties, including high electrical and thermal conductance, mesoporous metals offer a wider range of promising applications that cannot be achieved by other mesoporous materials.

In the past 10 years, my group has extensively studied various chemical approaches to achieve perfect mesoporous metallic architectures. Recently, we have proposed a micelle-assembly approach using diluted surfactant solutions for the preparation of mesoporous metals with accessible mesopores tunable over a wide range of sizes by selecting various surfactants and adding organic expanders. This process can be easily extended to the preparation of many mesoporous metals (e.g., Pt, Pd, Au, Cu) and other mesoporous alloys (e.g., PtPd, PtRu, PtAu), paving the way for novel electrode materials that can be applied in high-performance batteries. Due to such unique pore walls and high effective surface areas, the mesoporous metals obtained show remarkably high catalytic activity as electrocatalysts. Such a simple electrochemical design for mesoporous metals and alloys should contribute greatly to future applications, such as in microsensors, microbatteries, microbioactive materials, miniaturized devices, and beyond. Furthermore, this synthetic approach is expected to generate other metallic and semiconducting nanostructured films with architectures of technological importance.

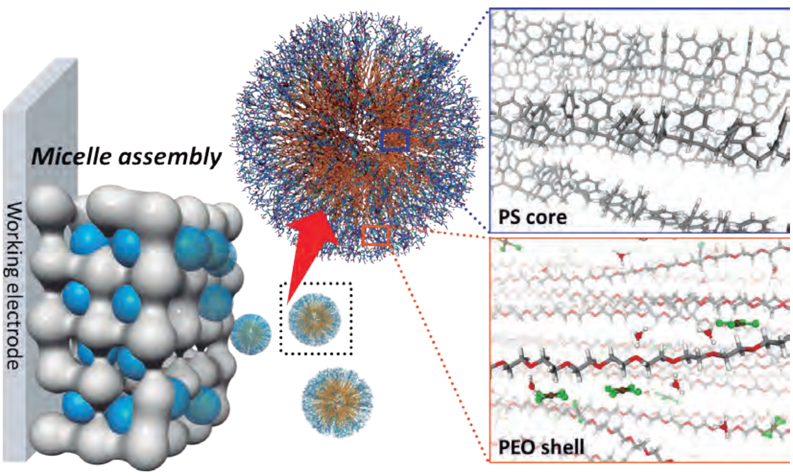

Fig. 1 Synthesis of metallic nanoporous material by the micelle assembly method (metal ions are coordinated in a diblock copolymer micelle consisting of polystyrene-polyethylene oxide (PS-PEO), and the metal ions are reduced on the micelles by the electrodeposition method).

Main Papers

1) "Surfactant-directed synthesis of mesoporous Pd films with perpendicular mesochannels as efficient electrocatalysts", C. Li, B. Jiang, N. Miyamoto, J.H. Kim, V. Malgras, Y. Yamauchi, *J. Am. Chem. Soc.* **137** (2015) 11558.
2) "Carbon materials: MOF morphologies in control", J. Tang, Y. Yamauchi, *Nature Chem.* **8** (2016) 638.
3) "Electrochemical synthesis of mesoporous gold films toward mesospace-stimulated optical properties", C. Li, Ö. Dag, T.D. Dao, T. Nagao, Y. Sakamoto, T. Kimura, O. Terasaki, Y. Yamauchi, *Nat. Commun.* **6** (2015) 6608.

27 Chiral sensing: novel chiral solvating agents for nondiastereomeric determination of enantiomeric excess

J. Labuta, S. Ishihara, K. Ariga, J. P. Hill

We developed a unique family of prochiral chiral solvating agents (pro-CSA) for the determination of enantiomeric excesses (*ee*) of a wide range of chiral analytes including carboxylic acids, alcohols, amines, and ketones using nuclear magnetic resonance (NMR) spectroscopy. This is made possible by the weak interaction and consequent rapid solution exchange between analyte and pro-CSA and can be considered as the sampling of the average chirality of the analyte in solution.

Chiral parameters of asymmetric compounds, including their absolute configurations and enantiomeric purity, are important in medical and pharmaceutical applications. Our achiral molecular system allows for the rapid analysis of enantiomeric purity in a wide range of organic substances, which not only facilitates the development of chiral drugs but also permits the study of asymmetric reaction pathways and chiral drug metabolism. These are important from the point of view of the widely used chiral catalysts and also suggest the use of our reagents for monitoring dynamic chiral transformations. Being achiral, our reagents are ideal for such purposes since they would not affect the outcome of such reactions in terms of their chirality.

ee can be determined by constructing a calibration curve where *ee* is proportional to a splitting in selected peaks in the NMR spectrum of the analyte[1,2]. This procedure allows for the rapid analysis of *ee* in, for instance, a pharmaceutical development scenario, where time-consuming high-performance liquid chromatography can be replaced by the commonly used NMR spectroscopy. In particular, the use of our pro-CSA should improve optimization times for asymmetric reaction development. Also, when a symmetrical molecule is adapted as an *ee* sensor, it has certain intrinsic advantages such as identical binding constants for each enantiomer, resulting in *ee* determination that is not obscured by kinetic resolution[2]. Our system can also be used to improve our understanding of important chirality principles such as majority rule and intermolecular chirality transfer. As a result of our careful molecular design, pro-CSA systems based on nanometric saddle-shaped tetrapyrroles for room-temperature NMR determination of *ee* values in a wide range of analyte types including acids, esters, amines (including amino acid derivatives), and ketones were established[3].

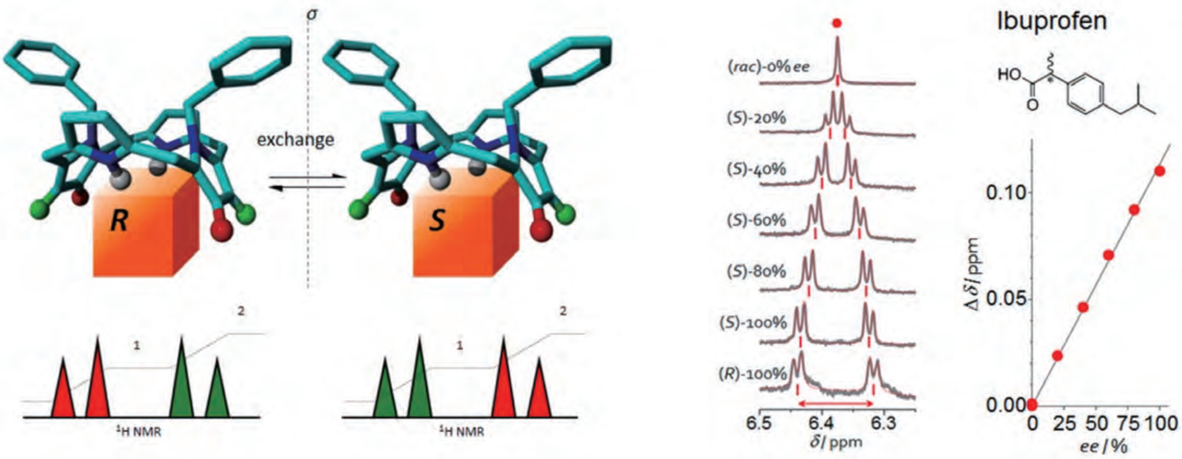

Fig. 1(Left)basic concept of *ee* sensing in achiral tetrapyrrole macrocyclic prochiral chiral solvating agents involving fast exchange of analyte molecules. **(Right)**data for Ibuprofen; splitting of NMR resonance is proportional to *ee* and a demonstration of its linearity.

Main Papers

1) "Nuclear magnetic resonance signaling of molecular chiral information using an achiral reagent", A. Shundo, J. Labuta, J.P. Hill, S. Ishihara, K. Ariga, *J. Am. Chem. Soc.* **131** (2009) 9494.
2) "NMR spectroscopic detection of chirality and enantiopurity in referenced systems without formation of diastereomers", J. Labuta, S. Ishihara, T. Šikorský, Z. Futera, A. Shundo, L. Hanyková, J.V. Burda, K. Ariga, J.P. Hill, *Nat. Commun.* **4** (2013) 3188.
3) "Chiral sensing using non-chiral porphyrins", J. Labuta, J.P. Hill, S. Ishihara, L. Hanykova, K. Ariga, *Acc. Chem. Res.* **48** (2015) 521.

28 Quantum transport of electric field-induced carriers in diamond

T. Yamaguchi, H. Takeya, Y. Takano

We observed quantum (Shubnikov-de Haas) oscillations in diamond for the first time. This was achieved by the preparation of atomically flat hydrogen-terminated diamond surfaces and the accumulation of high-density hole carriers due to the electric-field effect using an ionic liquid. The observation of quantum oscillations indicated a high-mobility metallic state of diamond, which will open up rich fields of research from fundamental physics to device applications.

Electronic applications of diamond have been anticipated in various fields owing to its excellent properties. As pure diamond is an insulator, the introduction of charge carriers is important for electronic applications. The most common method to introduce charge carriers is chemical doping. Heavy boron doping of diamond can induce a metallic state and even a superconducting state at low temperature. However, carrier scattering due to the high-density dopants leads to very low mobility. It is also predicted that the superconducting transition temperature is suppressed by the electronic disorder due to the heavy doping.

An alternative clean approach for introducing carriers is to use the electric-field effect. We prepared atomically flat hydrogen-terminated (111) surfaces of diamond and made high-density hole carriers to accumulate at the surfaces using an ionic-liquid-gated field-effect-transistor (FET) technique (Fig. 1(a)). This enabled us to obtain a high-mobility metallic state (Fig. 1(b)), in which we observed quantum (Shubnikov-de Haas) oscillations in diamond for the first time (Fig. 1(c))[1]. The quantum oscillations depend only on the magnetic field component perpendicular to the diamond surface, thus providing evidence of two-dimensional Fermi surfaces. The effective masses estimated from the temperature dependence of the oscillations are close to the cyclotron effective masses of the valence band maxima in diamond. The estimated scattering time indicates that the carrier mobility is locally as high as several thousand cm^2/Vs at low temperature. In addition, we also found spin-related anomalous magnetotransport phenomena for the electric field-induced carriers at the (100) surface of diamond[2].

The high-mobility metallic state and spin-dependent transport in diamond described here will open up the possibility of using diamond in the field of quantum transport and spintronics.

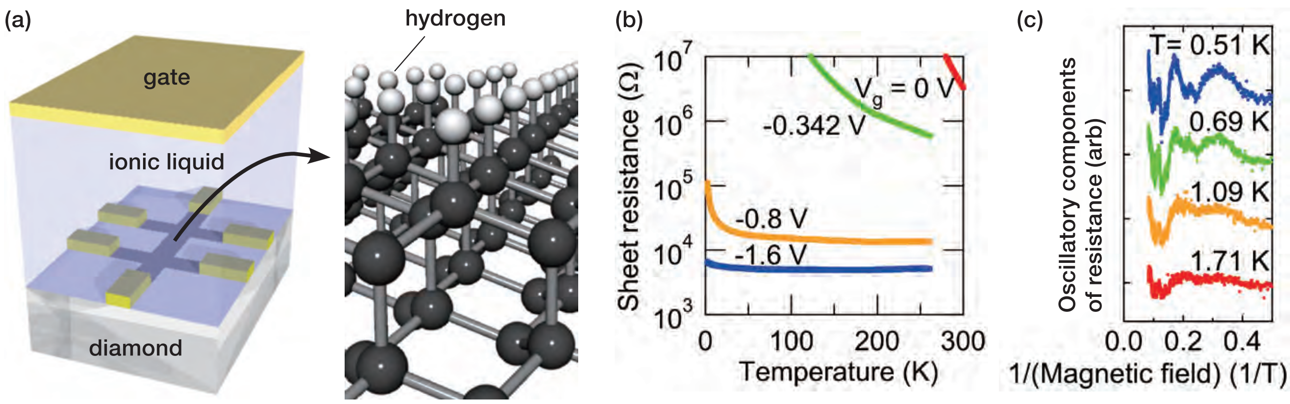

Fig. 1(a) Diamond FET using hydrogen-terminated surface and ionic-liquid gate. **(b)** Field-induced insulator–metal transition of diamond. **(c)** Shubnikov-de Haas oscillations of diamond.

Main Papers

1) “Quantum oscillations of the two-dimensional hole gas at atomically flat diamond surfaces”, T. Yamaguchi, H. Okazaki, K. Deguchi, S. Uji, H. Takeya, Y. Takano, H. Tsuboi, H. Kawarada, *Phys. Rev. B* **89** (2014) 235304.

2) “Spin-induced anomalous magnetoresistance at the (100) surface of hydrogen-terminated diamond”, T. Yamaguchi, Y. Sasama, M. Tanaka, H. Takeya, Y. Takano, T. Kageura, H. Kawarada, *Phys. Rev. B* **94** (2016) 161301(R).

29 Novel functional molecular liquids developed by alkyl-π engineering

T. Nakanishi

We developed novel ultimate-soft organic materials, i.e., room-temperature functional molecular liquids composed of a π-conjugated molecular unit bearing bulky, flexible branched alkyl chains. The studies of full-color tunable luminescent liquids and uncommon phase phenomena with the photoconducting property of liquid fullerenes are designed simply by controlling a balance of intermolecular interactions in the alkyl-π compounds, i.e., van der Waals and π–π interactions among adjacent molecules, or "alkyl-π engineering".

Apart from ordered fluid materials, i.e., liquid crystals, solvent-free room-temperature functional molecular liquids (FMLs)[1] attract attention as novel ultimate-soft organic materials. FMLs possess versatile processability, like geometry-independent coating and filling into narrow spaces via capillary action, and excellent stability under heat as well as great deformability. In addition, as a solvent function FMLs can accommodate other functional molecules within them and allow the adjustment of their properties in a predictable manner. Thus, FMLs can overcome many issues encountered in organic/polymeric substances for their practical use. Here, the molecular design principle of FMLs based on an alkylated-π molecular system as well as their luminescence and optoelectronic properties are introduced.

Our first molecular design was a luminescent π-conjugated core isolated by the attached bulky, flexible branched-alkyl chains, and the selected core is a blue-luminescent anthracene ((**1**), Fig. 1)[2]. Using this strategy, we achieved an intrinsic molecular optical property, i.e., luminescence, even in the solvent-free neat state showing almost the same optical features as a dilute solution. The liquid character of (**1**) allows for accommodation of energy-accepting emissive dopants, which inspires the creation of full-color luminescent liquid (Fig. 1(a)). In addition, the anthracene core is effectively wrapped with the bulky side chains, thus preventing its photodegradation.

Another research strategy is to direct the assembly of room-temperature liquid alkyl-C_{60} molecules (e.g., (**2**), Fig. 1). The C_{60} unit substituted with two branched alkyl chains on one side has an asymmetric molecular structure. Using additives that favor either the alkyl (n-alkane) or π-conjugated (pristine C_{60}) part, amorphous alkylated-C_{60} materials are assembled into ordered structures such as micelles and gel fibers with n-alkanes, and lamellar nanosheets with C_{60} (Fig. 1(b))[3]. The resulting gel fibers and lamellar nanosheets are composed of well-organized C_{60} moieties, thus changing them to photoconductive from the insulating disordered liquid state.

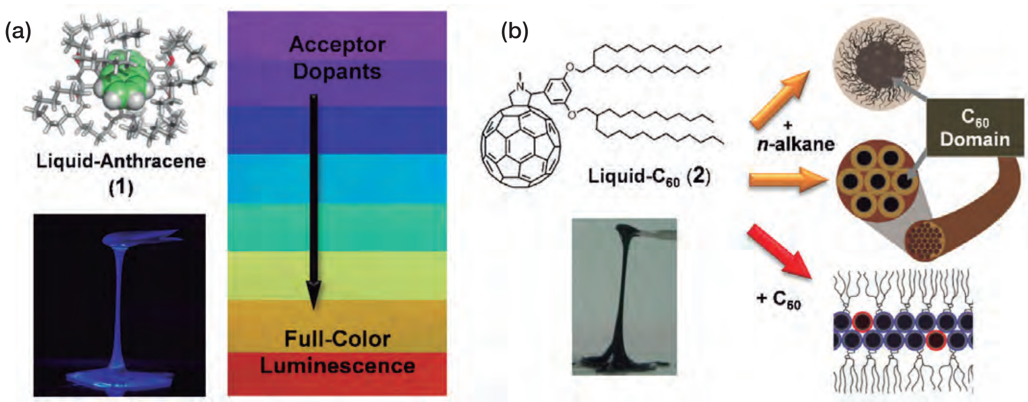

Fig. 1(a) An anthracene core isolated liquid molecule(**1**) and its blue photoluminescence that can be tuned for full-color emission with acceptor dopants. **(b)** Directed assembly of a liquid-C_{60} (**2**) with additives. Lamellar nanosheets formed with the addition of pristine C_{60} and micelles or gel fibers formed with n-alkane.

Main Papers

1) "Nonvolatile functional molecular liquids", S.S. Babu, T. Nakanishi, *Chem. Commun.* **49** (2013) 9373 (feature article, front cover picture).
2) "Nonvolatile liquid anthracenes for facile full-colour luminescence tuning at single blue-light excitation", S.S. Babu, M.J. Hollamby, J. Aimi, H. Ozawa, A. Saeki, S. Seki, K. Kobayashi, K. Hagiwara, M. Yoshizawa, H. Möhwald, T. Nakanishi, *Nat. Commun.* **4** (2013) 1969.
3) "Directed assembly of optoelectronically active alkyl-π-conjugated molecules by adding n-alkanes or π-conjugated species", M.J. Hollamby, M. Karny, P.H.H. Bomans, N.A.J.M. Sommerdijk, A. Saeki, S. Seki, H. Minamikawa, I. Grillo, B.R. Pauw, P. Brown, J. Eastoe, H. Möhwald, T. Nakanishi, *Nat. Chem.* **6** (2014) 690.

30 Silicon-doped metal oxide thin-film transistor for next-generation power-saving flat displays

K. Tsukagoshi, T. Nabatame

We developed a promising material for an oxide thin-film transistor (TFT) to produce next-generation power-saving flat displays. Our silicon (Si)-doped metal oxide TFT (SiM-OxTFT) behaves as a very stable, high-performance TFT with a significantly suppressed off-state current.

Amorphous Si or poly-Si film has customarily been used for pixel-switching TFTs in flat-panel displays. However, because of the very large off-state current in current TFTs, a new TFT model is needed to reduce power consumption. Furthermore, TFTs allowing greater mobility than amorphous Si are required to present high-resolution content. An amorphous metal oxide thin-film transistor (a-OxTFT) is a possible candidate for post-Si TFTs. Although indium-gallium-zinc-oxygen film is a potential candidate for the a-OxTFT, this film is unstable in actual production processes because its electric properties are extremely sensitive to oxygen absorption or desorption at the bonding sites adjacent to Zn atoms.

Indium oxide (InOx)-based semiconductors are expected to be useful switching elements in TFTs since they have high electron mobility originating from the direct overlap of the isotropic s orbitals of In atoms. To stabilize TFT characteristics by controlling the creation of oxygen vacancy (Vo), an oxygen-binding dopant is crucial in thin film. We therefore investigated a mechanism to create Vo to develop a high-performance TFT.

We found that the electric stability of the TFT is determined by the bond-dissociation energy of the dopant element in InOx film (Fig. 1). By incorporating a dopant with higher bond-dissociation energy, such as a Si atom, the film suppresses thermally active vacancies in the film. The basic performance properties of our original InSiO-OxTFT exceed that of current commercially produced TFTs. The material developed for our OxTFT will allow the production of very stable, high-performance TFTs with significant reduction of the off-state current to produce next-generation power-saving flat displays.

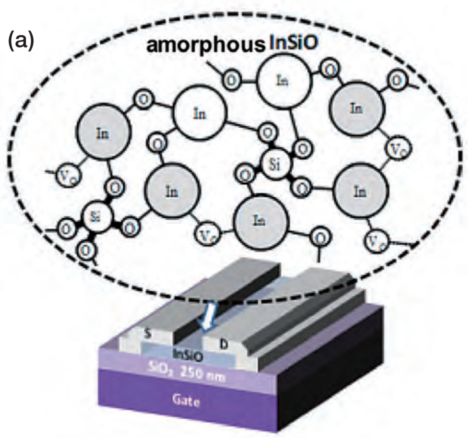

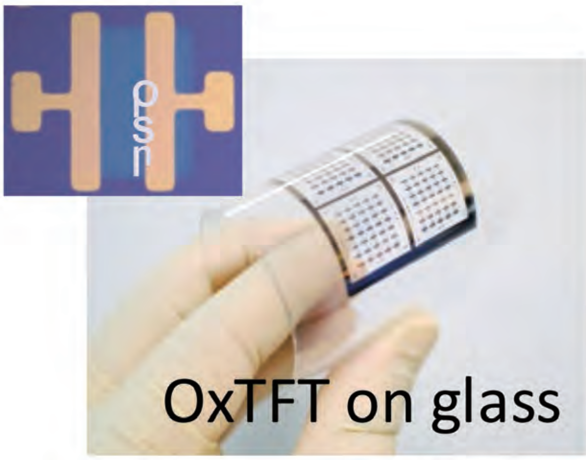

Fig. 1(a) Schematic of stable amorphous In_2O_3-based TFTs by incorporating SiO_2 with illustration of Vo suppression by incorporating SiO_2. **(b)** Photo of InSiO-OxTFTs on a flexible glass substrate.

Main Papers

1) "Thin-film transistors fabricated with low temperature process based on Ga- and Zn-free amorphous oxide semiconductor", S. Aikawa, P. Darmawan, K. Yanagisawa, T. Nabatame, Y. Abe, K. Tsukagoshi, *Appl. Phys. Lett.* **102** (2013) 102101.
2) "Stable amorphous In_2O_3-based thin-film transistors by incorporating SiO_2 to suppress oxygen vacancies", N. Mitoma, S. Aikawa, X. Gao, T. Kizu, M. Shimizu, M.-F. Lin, T. Nabatame, K. Tsukagoshi, *Appl. Phys. Lett.* **104** (2014) 102103.
3) "Dopant selection for control of charge carrier density and mobility in amorphous indium oxide thin-film transistors: Comparison between Si- and W-dopants", N. Mitoma, S. Aikawa, W. Ou-Yang, X. Gao, T. Kizu, M.-F. Lin, A. Fujiwara, T. Nabatame, K. Tsukagoshi, *Appl. Phys. Lett.* **106** (2015) 042106.

31 New high-k materials for future Ge field-effect transistors

T. Chikyow, T. Nagata, Y. Yamashita

Direct contact of high-k oxide on a Ge substrate was demonstrated with a TiO_2 buffer layer. Rutile TiO_2 was grown on p-type (100) Ge substrates at 420°C. During the deposition, originally formed GeO_2 was decomposed, and Ge diffusion to TiO_2 was observed. By optimizing the growth conditions, Ge diffusion was minimized. HfO_2 was subsequently deposited on this TiO_2 to make HfO_2/TiO_2 stacked high-k layers. The electric property showed reduced leakage current, although a large threshold voltage shift was observed.

The scaling of large-scale integrated circuits in logic and memory devices continues, and gate length will be in 7-nm node by 2020. To enhance mobility for higher-speed switching, alternative substrates are considered. The leading candidate is Ge due to higher carrier mobility. However, direct contact of high-k oxide on Ge was not possible due to thermally unstable GeO_2. The scavenging method is not applicable for GeO_2 elimination because this method requires higher process temperature[1,2].

For direct contact of oxide with Ge, TiO_2 was selected due to its heat of formation. GeO_2 bonding energy is 57 kcal/bond and that of TiO_2 is 112.9 kcal/bond. The value is almost half of GeO_2 heat of bonding, meaning that if oxygen-deficient TiO_x contacts GeO_2, TiO_2 forms by GeO_2 reduction. TiO_2 also has a higher dielectric property.

After degreasing and surface cleaning with hydrogen fluoride solution, a Ge substrate was installed in a vacuum chamber and heated to 500°C to remove the surface oxide layer. Subsequently, TiO_2 was deposited on the surface in an oxygen atmosphere of 10−6 Torr. The TiO_2 film was characterized by X-ray diffraction (XRD) and epitaxial rutile TiO_2 growth was observed (Fig. 1)[2]. An interfacial layer of GeO_2 was not observed in X-ray photoelectron spectroscopy, and an abrupt interface of TiO_2/Ge was demonstrated. However, some Ge was involved in TiO_2, and the effect of Ge was minimized by controlling the growth temperature[3]. HfO_2 was deposited on TiO_2 to fabricate a gate stack structure, followed by Pt deposition. The metal–oxide semiconductor capacitor did not show hysteresis, meaning that the fixed charge or interface trap density was not high, although a large shift in threshold voltage occurred (Fig. 1(d)). The equivalent oxide thickness (EOT) was estimated to be 0.78 nm, the lowest value of a high-k insulator on Ge.

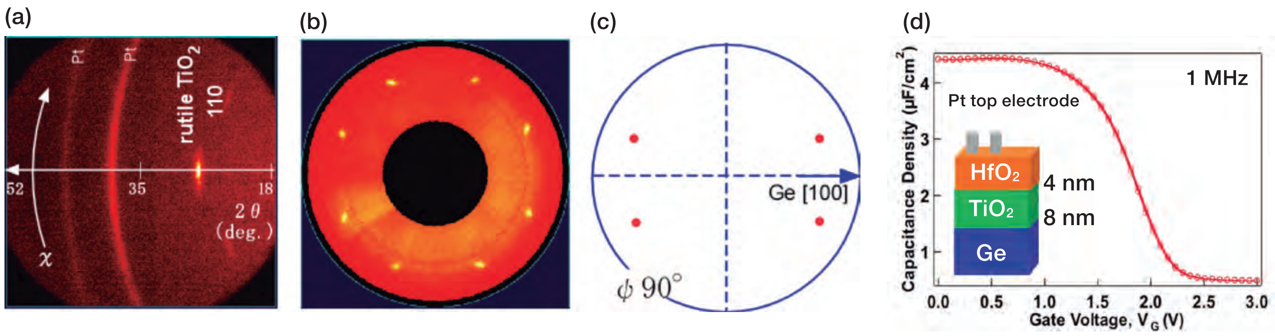

Fig. 1(a) 2D-XRD pattern and **(b)** pole figure image of 30 nm thick TiO_2 on Ge substrate deposited at 420 ℃ **(c)** Theoretical pole figure image of the [101] plane for rutile TiO_2.These results show that rutile TiO_2 was epitaxially grown on Ge substrate. **(d)** C–V characterization showed less hysteresis. EOT was estimated to be 0.78 nm.

Main Papers

1) "Reduction of Interfacial SiO_2 at HfO_2/Si interface with Ta_2O_5 Cap", K. Kobashi, T. Nagata, T. Nabatame, A. Ogura, T. Chikyow, *J. Appl.Phys.* **114** (2013) 014106.
2) "Ge incorporated epitaxy of (110) rutile TiO_2 on (100) Ge single crystal at low temperature by pulsed laser deposition", T. Nagata, K. KOBASHI, Y. Yamashita, H. Yoshikawa, C. Paulsamy, Y. Suzuki, T. Nabatame, A. Ogura, T. Chikyow, *Thin Solid Films* **591** (2015) 105.
3) "Thin-film growth of (110) rutile TiO_2 on (100) Ge substrate by pulsed laser deposition", Y. Suzuki, T. Nagata, Y. Yamashita, A. Ogura, T. Chikyow, *Jpn. J. Appl. Phys.* **55** (2016) 06GG06.

32 Printed electronics: spontaneous patterning of high-resolution electronics

T. Minari

Fully printed electronics on a flexible substrate have attracted considerable interest owing to their high compatibility and ease of integration. We developed an ultra-high-resolution printing technique based on fluidic self-assembly, which enables selective deposition of a metal nanoparticle (NP) ink with a 1-µm feature size. We also employed a room-temperature fabrication procedure to prevent undesired distortion of the heat-sensitive, flexible substrate. The technique thereby allows the large-scale fabrication of flexible electronics with 1-µm resolution at low cost.

Patterning of functional materials into microstructures has received increasing interest for optical, electronic, biological, and sensory applications. In particular, spontaneous patterning of electronic circuits is presently considered the most promising, nonlithographic, mold-free approach for large-area plastic devices.

We proposed the spontaneous self-assembly of metal NPs as a novel fabrication process for semiconductor devices, which enables the homogeneous integration of complex, high-resolution electronic circuits even on large-scale, flexible, transparent substrates[1-3]. First, we achieved the all-solution-processed fabrication of organic thin-film transistors (OTFTs) using the surface wettability contrast[1]. Vacuum ultraviolet (VUV, $\lambda < 200$ nm) irradiation of the hydrophobic polymer surface through a photomask precisely rendered the selected surface into highly wettable regions, which spontaneously guided a metal NP ink into the desired structure of electronic circuits. Next, we succeeded in room-temperature fabrication of fully printed OTFT devices using a novel gold NP ink consisting of a metal core surrounded by the conductive planner molecules as the ligand[2]. Moreover, we improved the resolution of our printing technique to fabricate short-channel OTFTs by employing parallel VUV (PVUV)[3]. The wettability contrast with sharply defined boundaries by PVUV allows fabricating a series of circuit lines and gaps with widths down to 1 µm. The use of room-temperature processes throughout the fabrication prevented the undesired distortion of the heat-sensitive, flexible substrate due to thermal annealing, which allowed the homogeneous fabrication of devices with ultra-high accuracy even for a large area. The spontaneous patterning also allowed selective deposition of charge injection layers, which reduced the contact resistance to 1.5 kΩcm. As a result, the spontaneously solution-processed OTFTs exhibited high field-effect mobility values of 0.3 and 1.5 $cm^2\ V^{-1}\ s^{-1}$ with channel lengths of 1 and 5 µm, respectively, which is comparable to that of vacuum-deposited devices.

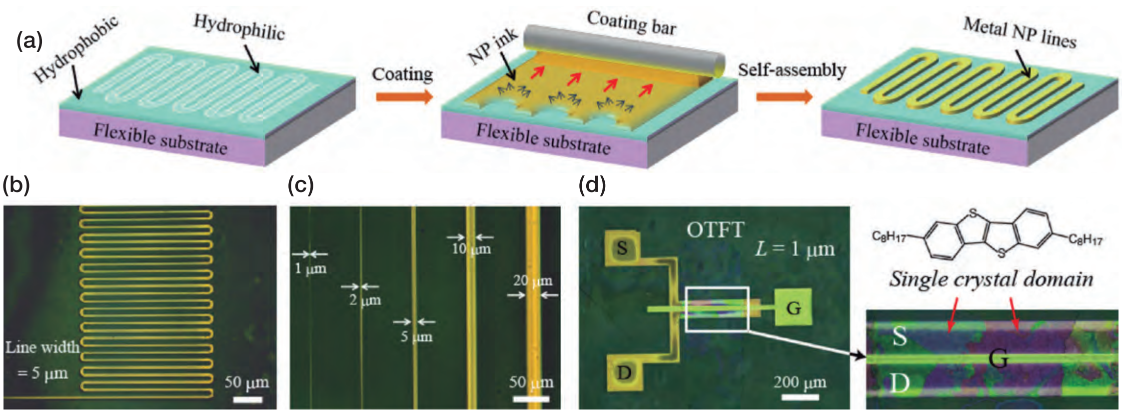

Fig. 1(a) Spontaneous patterning of high-resolution circuits by fluidic self-assembly. **(b), (c)** Optical microscope images of patterned Au electrodes. **(d)** Fully-printed OTFTs with 1-µm channel length.

Main Papers

1) "Controlled self-assembly of organic semiconductors for solution-based fabrication of organic field-effect transistors", T. Minari, C. Liu, M. Kano, K. Tsukagoshi, *Adv. Mater.* **24** (2012) 299.
2) "Room-temperature printing of organic thin-film transistors with pi-junction gold nanoparticles", T. Minari, Y. Kanehara, C. Liu, K. Sakamoto, T. Yasuda, A. Yaguchi, S. Tsukada, K. Kashizaki, M. Kanehara, *Adv. Funct. Mater.* **24** (2014) 4886.
3) "Spontaneous patterning of high-resolution electronics via parallel vacuum ultraviolet", X. Liu, M. Kanehara, C. Liu, K. Sakamoto, T. Yasuda, J. Takeya, T. Minari, *Adv. Mater.* **28** (2016) 6568.

33 Novel concepts for III-V nitride optoelectronic devices

L. Sang

Benefiting from the wide, adjustable, direct bandgaps, high breakdown voltage, and high carrier mobilities, the III-V nitride semiconductor (GaN, InN, AlN, and their ternary and quaternary alloys) is not only a potential candidate for high-performance optical devices but also for high-power, and high-frequency electronic devices. However, there are still challenges in high-quality film growth and effective *p*-type doping, which hinders the development of nitride devices. Our research on InGaN-based ultraviolet photodiodes, intermediate-band solar cells, and *p*-channel field-effect transistors with a InGaN/GaN heterojunction structure is introduced here.

The reevaluation of the bandgap energy of InN extends the basic absorption wavelength of III-V nitride semiconductors from the infrared (InN at 0.65 eV) through visible and ultraviolet (UV) (GaN at 3.42 eV) to the deep UV range (AlN at 6.2 eV), which covers nearly the full spectrum. This unique property makes them promising candidates for photoelectricity energy-conversion devices, such as visible-blind photodiodes, solar cells, and LEDs. On the other hand, compared with Si and GaAs semiconductors, III-V nitrides have a higher breakdown voltage, larger saturation velocity, higher carrier mobility, and higher thermal stability, which are suitable for next-generation high-power, and high frequency electronic devices. However, the development of nitride optoelectronics is still far from ideal due to issues involving film epitaxy, effective *p*-type doping, and poor device concepts.

To solve the above problems, we proposed a unique high-pressure growth method for the epitaxial growth of In-rich InGaN and achieved *p*-type conductivity using a polarization-induced doping method. Based on the high-quality films, novel devices were developed. For example, visible-blind photodetectors with the highest spectrum selectivity (UV/visible ratio $>10^6$) were developed using CaF_2 as the insulator. For the InGaN solar cells, we first proposed and experimentally produced intermediate-band transitions using multiple strain-modulated quantum-dot structures and successfully extended the photoresponse spectrum from deep UV to the near-infrared region, which is the widest ever reported. The first *p*-channel metal–oxide–semiconductor field-effect transistors (MOSFETs) with InGaN/GaN heterojunctions was also developed, which can be operated at temperatures as low as 8 K. This work opens a promising route for the development of nitride one-chip complementary integrated circuits (ICs).

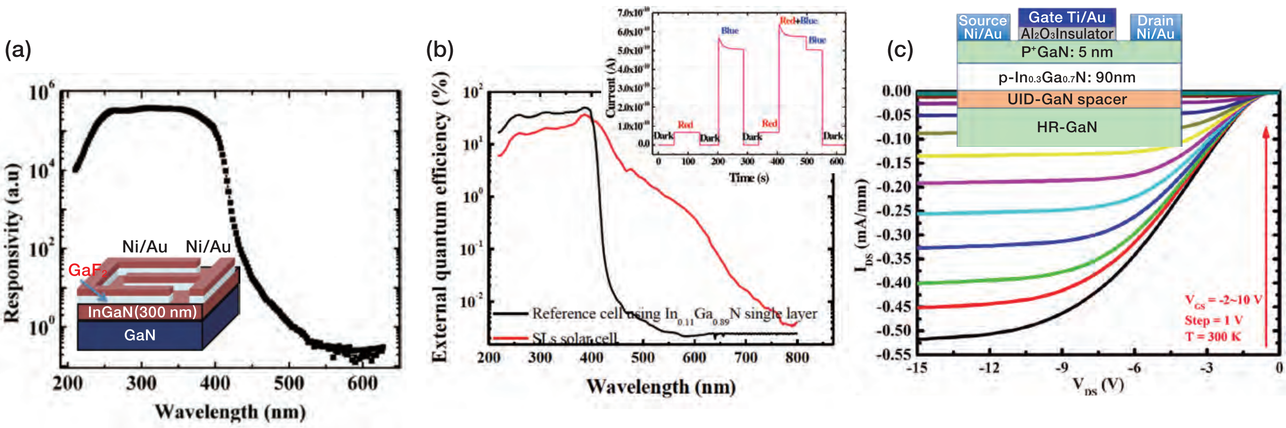

Fig. 1(a) High-performance visible-blind photodetectors. **(b)** The first nitride intermediate-band solar cells. **(c)** The first p-channel InGaN/GaN MOSFETs for complementary-power ICs.

Main Papers

1) "Multilevel intermediate-band solar cell by InGaN/GaN quantum dots with a strain-modulated structure", L. Sang, M. Liao, Q. Liang, M. Takeguchi, B. Dierre, T. Sekiguchi, Y. Koide, M. Sumiya, *Adv. Mater.* **26** (2014) 1414.

2) "Arbitrary multicolor photodetection by hetero-integrated semiconductor nanostructures", L. Sang, J. Hu, R. Zou, Y. Koide, M. Liao, *Sci. Rep.* **3** (2013) 2368.

3) "Enhanced performance of InGaN solar cell by using a super-thin AlN interlayer", L. Sang, M. Liao, N. Ikeda, Y. Koide, M. Sumiya, *Appl. Phys. Lett.* **99** (2011) 161109.

34 Multifunctional electron tunneling devices with molecular quantum dots

R. Hayakawa, Y. Wakayama

Precise control of electron tunneling is critical for power-saving electronic devices. Our purpose was to develop electron tunneling devices based on a variety of molecular functions. Functional molecules were integrated into a Si-based architecture, aiming to bridge the gap between fundamental quantum effects and practical device engineering. Here, we demonstrate the fundamental mechanism, multilevel tunneling, and optical control of electron tunneling. These results were achieved by taking advantage of organic molecules as quantum dots.

For practical development, quantum dots for electron tunneling devices should be well designed on a nanometer scale. For example, the size of the quantum dots should be a few nanometers to allow room-temperature operation. Size uniformity is another important factor for fine control of the threshold voltage (V_{th}). To meet these requirements, we adopted organic molecules as quantum dots. Fullerene (C_{60}) molecules were embedded in a metal–oxide semiconductor (MOS) structure (Fig. 1(a)). Staircases in current-voltage curves were observed in a double-tunneling junction consisting of Au/Al_2O_3/C_{60}/SiO_2 multilayers on Si(100) substrates. Here, C_{60} and Al_2O_3 and SiO_2 layers served as intermediate electrodes and tunneling barriers, respectively. We elucidated that the observed staircases were attributed to resonant tunneling through the empty and occupied energy levels of the C_{60} molecules. The energy diagram is shown in Fig. 1(b). These results clearly indicate that the V_{th} for electron tunneling can be tuned precisely as requested by designing the molecular structure.

We applied this mechanism to various functional tunneling manipulations, i.e., multilevel tunneling and optical switching of electron tunneling. First, heterogeneous phthalocyanine molecules were embedded in the MOS structure. Multilevel tunneling according to the energy levels of the respective phthalocyanine molecules was successfully observed. Second, a reversible photochromic reaction (open-ring/closed-ring isomerization) of diarylethene was applied for optical switching. Optical control of electron tunneling was achieved upon UV and visible light irradiation with a memory effect.

Importantly, our device configuration is compatible with that of a conventional MOS-field-effect transistor device, and therefore these results demonstrate the potential practical use of molecules for energy-saving tunneling devices in Si-based devices, such as single-electron memory, multilevel tunneling switching devices, and photon–electron converters.

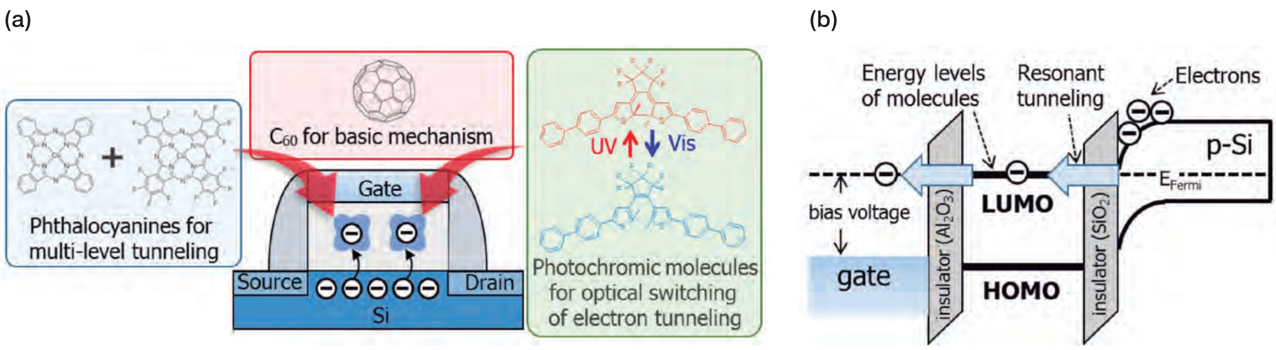

Fig. 1(a) Device and molecular structures. (b) Energy-level diagram showing resonant tunneling.

Main Papers

1) "Single-electron tunneling through molecular quantum dots in metal-insulator-semiconductor structure", R. Hayakawa, N. Hiroshiba, T. Chikyow, Y. Wakayama, *Adv. Func. Mater.* **21** (2011) 2933.
2) "Photoisomerization-induced manipulation of single-electron tunneling for novel Si-based optical memory", R. Hayakawa, T. Chikyow, Y. Wakayama, K. Higashiguchi, K. Matsuda, *ACS Appl. Mater. Interfaces* **5** (2013) 11371.
3) "Multilevel operation of single-electron tunneling with binary molecules in a metal-insulator-semiconductor configuration", H.-S. Seo, R. Hayakawa, T. Chikyow, Y. Wakayama, *J. Phys. Chem. C* **118** (2014) 6467.

35 Photothermal energy conversion with novel plasmonics and metamaterials

T. Nagao, S. Ishii Co-workers: T. D. Dao, T. Yokoyama

We developed a new class of nanomaterials/nanodevices with high photothermal conversion efficiency based on plasmonics and metamaterials. A new methodology for choosing appropriate compound materials was adopted to permit full-solar spectrum absorption for solar-heat generation. Our metamaterial perfect absorber can be applied for narrow-band infrared (IR) light sources with low energy consumption and for spectroscopic IR sensors, opening the way for new usages and demand in industrial quality control as well as in daily life.

The technology for amplifying, confining, and scattering light at nanoscale is strongly desired as a key technology in communication, optical sensing, and energy harvesting. Plasmonics and metamaterials are now accepted as useful paradigms to achieve desirable optical properties that are not possible with natural materials. Through this approach, we have been developing various materials and devices, as briefly introduced below.

We demonstrated through numerical calculations that nanoparticles of transition metal nitrides (e.g., TiN) and carbides (e.g., TaC) absorb sunlight very efficiently and confirmed experimentally that, when dispersed in water, nanoparticles of these materials quickly raise water temperature and generate vapor[1]. Since these nanoparticles exhibit broadband plasmon resonances that nearly overlap with the solar spectrum, their sunlight absorption efficiency is higher than that of gold and carbon nanoparticles. These nanoparticles can be applied for heating (Fig. 1(a)) and distillation of water through sunlight illumination.

IR metamaterial perfect absorbers, which can absorb 100% of IR radiation, have great potential for use in various applications such as sensing trace amounts of molecules and electrical power generation by absorbing thermal radiation. We developed IR metamaterial narrowband perfect absorbers using metal–oxide–metal structures in combination with alternative plasmonic materials such as Al, Mo, and TiN. Our perfect absorbers can perform as wavelength-selective IR light sources following Kirchhoff's law of thermal radiation[2,3]. We also developed spectroscopic IR detectors using the IR metamaterial perfect absorbers for wavelength-selective IR light detection[4] as shown in Fig. 1(b). Our IR detector can extend the usage of IR sensors to environmental sensors for robot cars, human motion sensors in hospitals, and material sensors and toxicology testing for homeland security.

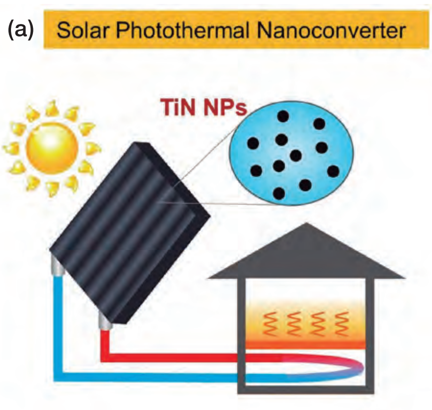

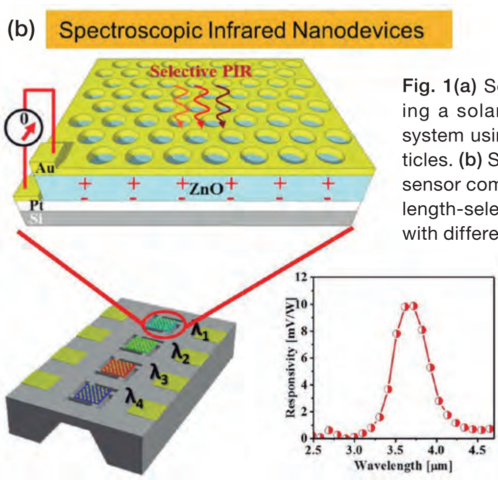

Fig. 1(a) Schematic showing a solar water-heating system using TiN nanoparticles. **(b)** Spectroscopic IR sensor composed of wavelength-selective IR sensors with different wavelengths.

Main Papers

1) "Titanium Nitride Nanoparticles as Plasmonic Solar Heat Transducers", S. Ishii, R. P. Sugawaneshwar, T. Nagao, *J. Phys. Chem. C* **120** (2016) 2343.
2) "Hole Array Perfect Absorbers for Spectrally Selective Mid-Wavelength Infrared Pyroelectric Detectors", T. D. Dao, S. Ishii, T. Yokoyama, T. Sawada, R. P. Sugawaneshwar, K. Chen, Y. Wada, T. Nabatame, T. Nagao, *ACS Photonics*, **3** (2016) 1271.
3) "Spectrally Selective Mid-Infrared Thermal Emission from Molybdenum Plasmonic Metamaterial Operated up to 1000 ℃", T. Yokoyama, T. D. Dao, K. Chen, S. Ishii, R. P. Sugawaneshwar, M. Kitajima, T. Nagao, *Adv. Opt. Mat.* **4** (2016) 1987.
4) "Infrared Perfect Absorbers Fabricated by Colloidal Mask Etching of Al–Al2O3–Al Trilayers", T. D. Dao, K. Chen, S. Ishii, A. Ohi, T. Nabatame, M. Kitajima, T. Nagao, *ACS Photonics*, **2** (2015) 964.

36 Graphene-based single-electron devices

S. Moriyama

We developed quantum nanodevices such as single-electron transistors in graphene, consisting of an isolated single atomic layer of graphite, as unrolled carbon nanotubes. The discovery of novel electron-transport characteristics in single- and several-layer graphene demonstrates that it is an attractive two-dimensional conducting material, not only as a new field in low-dimensional physics but also as building blocks of novel quantum nanodevices.

Quantum dots are expected to function as basic structures for operating single-electron electronics and quantum bits, which are the basic elements of quantum information processing, and research is being conducted on various materials. In particular, scalability that can be extended from a demonstration of single-device operation to a large number of integrated quantum circuits is important. Graphene, a single layer of graphite, is one attractive material suitable for these conditions.

We demonstrated quantum-dot devices in a graphene-based two-dimensional system. Graphene nanostructures can be fabricated by carving them out of the graphene sheet. Using high-resolution electron-beam lithography, we patterned a thin resist that protected chosen areas during oxygen plasma etching and allowed us to carve graphene into the desired geometry. Fig. 1(a) shows a scanning electron microscope image of the fabricated double-quantum-dot device in a triple-layer graphene. The device consisted of two triangular-shaped islands as quantum dots, connected via two short constrictions to wide source and drain regions, as shown schematically in Fig. 1(b). Three lateral graphene side gates were fabricated close to the active graphene structure.

Low-temperature transport results revealed that the device acts as single-electron transistors in which the electrons flow through the quantum dots one by one. Fig. 1(c) shows an experimental charge stability diagram. Honeycomb structures in this mapping, which are characteristic of coupled quantum dots, are clearly observed. In our research, charge stability diagrams with tunable interdot tunnel-coupling were observed. We also demonstrated magnetic field-induced quantum dots in single-layer graphene.

The research showed the possibility of developing integrated nanodevices using graphene. It is expected to contribute to progress in single-electron electronics and the development of novel functional nanoelectronics, so-called “Beyond CMOS” including quantum information processing.

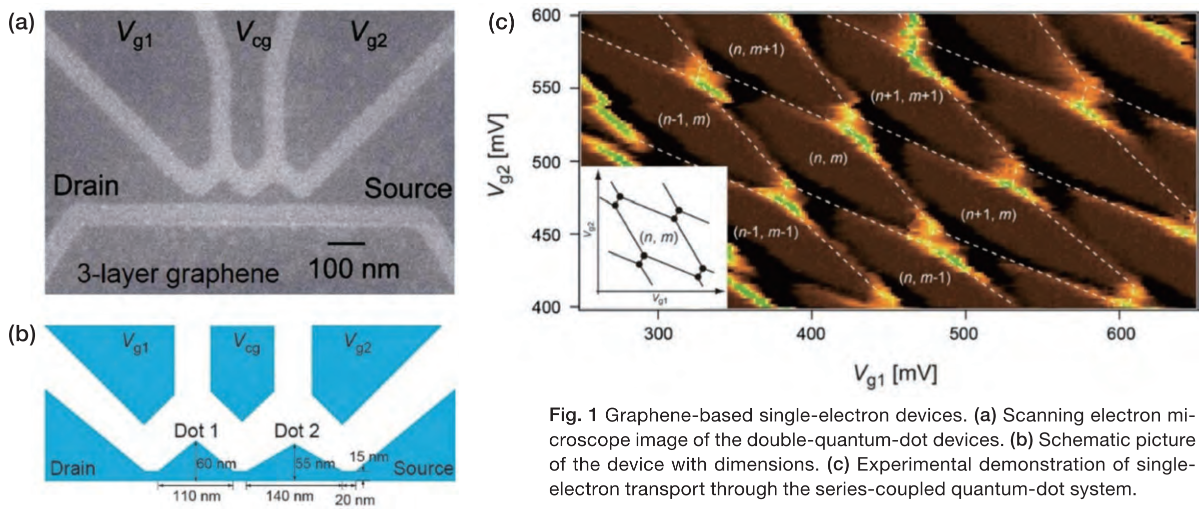

Fig. 1 Graphene-based single-electron devices. **(a)** Scanning electron microscope image of the double-quantum-dot devices. **(b)** Schematic picture of the device with dimensions. **(c)** Experimental demonstration of single-electron transport through the series-coupled quantum-dot system.

Main Papers

1) “Coupled quantum dots in a graphene-based two-dimensional semimetal,” S. Moriyama, D. Tsuya, E. Watanabe, S. Uji, M. Shimizu, T. Mori, T. Yamaguchi, K. Ishibashi, *Nano Lett.* **9** (2009) 2891.
2) “Fabrication of quantum-dot devices in graphene,” S. Moriyama, Y. Morita, E. Watanabe, D. Tsuya, S. Uji, M. Shimizu, K. Ishibashi, *Sci. Technol. Adv. Mater.* **11** (2010) 054601.
3) “Field-induced confined states in graphene,” S. Moriyama, Y. Morita, E. Watanabe, D. Tsuya, *Appl. Phys. Lett.* **104** (2014) 053108.

37 Exploring new frontiers of materials science in terms of topology

T. Kawakami, X. Hu

Because uncertainty caused by quantum fluctuations is unavoidable at nanometer scales, new schemes have to be created for achieving novel functionalities in nano systems. In order to take up this challenge, we are developing a new approach coined "topological nanoarchitectonics". One example is the quest for Majorana bound states (MBS) in topological superconductors, which can be exploited for robust quantum computation.

Topology is a concept in mathematics, which describes the way of connection of an object invariant upon continuous deformation. Recently it was noticed that topology can be defined in electronic states of materials, which ensures stable quantum properties desired for important implications. Topological superconductivity is unique because it accommodates MBS robust against noises.

Majorana fermion is special because it is equivalent to its own antiparticle, which was proposed to explain the charge-neutral neutrino. While Majorana fermion remains illusive as an elementary particle even after 80 years of research, in the past decade it was discussed that quasiparticles in topological superconductors behave similarly to Majorana fermions. The MBS at superconducting vortices can achieve non-Abelian statistics useful for quantum computation. A world-wide race is underway to confirm their existence.

We focused on the heterostructure of s-wave superconductor $NbSe_2$ and topological insulator Bi_2Te_3 shown in Fig. 1. Solving Bogoliubov-de Gennes equation, we revealed that two MBS appear at the top surface and interface inside the vortex. We evaluated the density of states (DOS) of quasiparticles as a function of bias energy and distance from vortex center, and by comparing our numerical results with a scanning tunneling microscopy/scanning tunneling spectroscopy (STM/STS) experiment, we concluded that MBS had been realized.

Because of the finite resolution of STM/STS, the spectrum obtained in experiments is continuous and thus MBS could not be identified as isolated quantum states. We noticed that there is a unique spin dependence in the quasiparticle wavefunction, and revealed theoretically that the ratio between DOSs in spin-up and -down channels should exhibit a checkerboard-type pattern as displayed in Fig. 1. Adopting a spin-polarized STM tip, one can resolve clearly the zero-energy MBS. Hopefully MBS will be captured in the near future as isolated quantum states, and exploited for robust quantum computation.

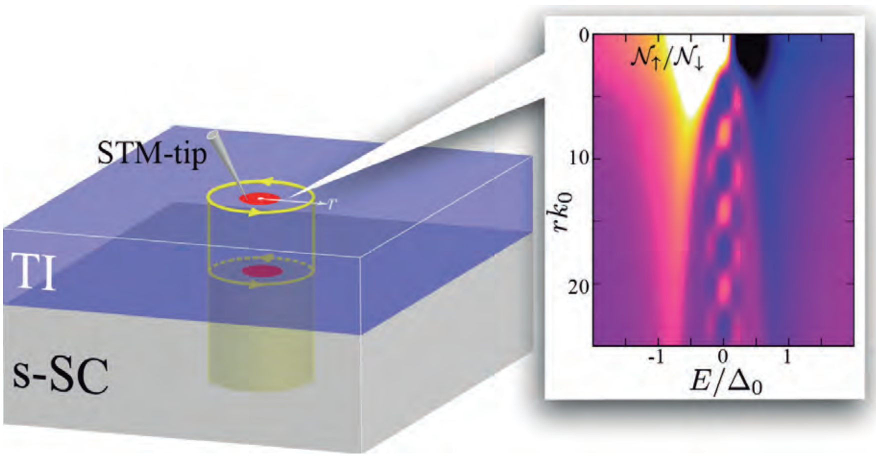

Fig. 1 Schematic of a topological superconductor with a vortex accommodating two MBS, and the calculated spin-resolved spectrum of quasiparticle excitations inside the vortex.

Main Papers

1) "Evolution of density of states and a spin-resolved checkerboard-type pattern associated with the Majorana bound state", T. Kawakami and X. Hu, *Phys. Rev. Lett.* **115** (2015) 177001 (cover story).
2) "Quantum anomalous Hall effect and topological electronic states", H.-M. Weng, R. Yu, X. Hu, X. Dai and Z. Fang, *Adv. Phys.* *64* (2015) 227 (review article).
3) "Manipulation of Majorana fermions by point-like gate voltage in the vortex state of a topological superconductor", Q.-F. Liang, Z. Wang, and X. Hu, *Europhys. Lett.* **99** (2012) 50004 (editors' choice).

38 Laser control of nondissipative electric current in topological materials

J. Inoue

We constructed a theoretical framework that enables discussion of matter and intense-light interaction, which is beyond the scope of conventional theories. Our theory predicts that laser irradiation can induce a phase transition in topological material, thereby leading to control of nondissipative electric current by tuning laser amplitude.

The traditional use of optics in material science is measuring optical constants of materials, and in this way the former has significantly contributed to the latter. However, optics can further impact material science from various perspectives, as we theoretically clarified.

The potential of optics can be recognized by going beyond conventional theoretical treatment based on a perturbation method. This must begin by building a theoretical framework that can handle interactions between matter and high-intensity light. We employed the Floquet theorem, known in mathematics, to take matter–light interaction up to infinite order into account and successfully developed it as a photo-steering theory[1)–3)]. To demonstrate the power of the theory, we selected low-dimensional insulators as target material and confirmed that laser light can change their topological nature, manifested as an electron transport phenomenon[2,3)]. In a specific case, nondissipative electric current can be controlled by changing the laser amplitude applied (Fig. 1), where an elegant fusion of physics and geometry is relevant. This phenomenon is a class of topological phase transition, one of the hottest research topics for this decade. The idea used in our theoretical work has, in conjunction with other theorists' work, opened the door for a new subbranch in physics, called Floquet engineering, which was one consideration in awarding the Nobel Prize for Physics in 2016.

The stance we take toward theoretical studies, in contrast to proposals for future materials based on first-principles calculation, is yet another contribution to material science.

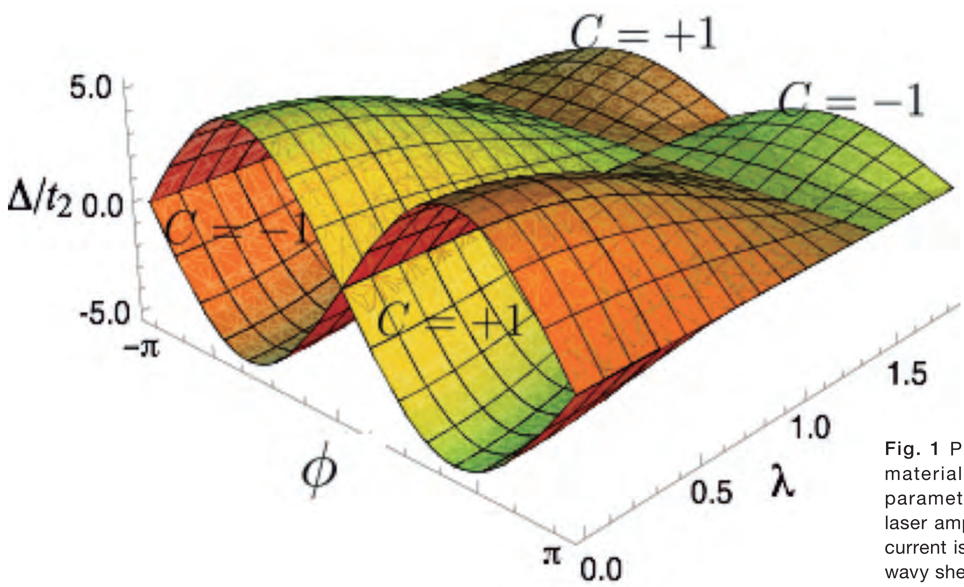

Fig. 1 Phase diagram of topological material considered in this study. A parameter lambda is proportional to laser amplitude. Nondissipative electric current is possible in regions within two wavy sheets. One can enter and exit the regions by changing laser amplitude.

Main Papers

1) "Photoinduced adiabatic state transfer in low-dimensional electronic systems", J. Inoue, *Phys. Rev. B* **81** (2010) 125412.
2) "Photoinduced transition between conventional and topological insulators in two-dimensional electronic systems", J. Inoue, A. Tanaka, *Phys. Rev. Lett.* **105** (2010) 017401.
3) "Adiabatic photo-steering theory in topological insulators", J. Inoue, *Sci. Technol. Adv. Mater.* **15** (2014) 064403.

39 Nature of the Mott transition

M. Kohno

The nature of the Mott transition is theoretically clarified: the Mott transition is characterized by freezing of the charge degrees of freedom, whereas the spin degrees of freedom remain active. This characteristic is contrasted with the conventional picture where the Mott transition was considered to be characterized in terms of single particles carrying spin and charge.

The effects of strong electronic correlations, causing various properties of materials, are central topics in condensed-matter physics. The most remarkable phenomenon caused by such correlations is the Mott transition: electrons behaving like single particles carrying spin and charge in a metal become those exhibiting spin-charge separation in a Mott insulator. The Mott transition has attracted considerable attention in relation to high-temperature superconductivity in cuprates near the Mott transition.

As conventional pictures of the Mott transition, two possibilities were considered. (1) The Mott transition can be understood like a metal-insulator transition for a band insulator (semiconductor), where holes disappear from a band edge with the band structure essentially unchanged. (2) Because the Mott transition is caused by strong electronic correlations, it occurs due to divergence of the effective mass of electrons (quasi-particles), thus narrowing the effective bandwidth of the quasi-particles. In either case, the Mott transition was considered to be characterized in terms of single particles.

To clarify the nature of the Mott transition, the one-dimensional Hubbard model, the simplest model exhibiting the phenomenon, was studied using exact solutions and numerical methods[1)]. This model showed that the Mott transition is characterized by freezing of the charge degrees of freedom, whereas the spin degrees of freedom remain active. Although the spectral weight of the low-energy electron-addition excitation fades toward the Mott transition, the dispersion relation of the electron excitation continuously transforms into that of the magnetic excitation of the Mott insulator with the momentum shifted by Fermi momentum (Fig. 1)[1)]. This was also seen in the two-dimensional Hubbard model using numerical methods[2)] and supported by general arguments in the small-doping limit[3)]. Thus, this characteristic reflecting the spin-charge separation of a Mott insulator is the nature of the Mott transition.

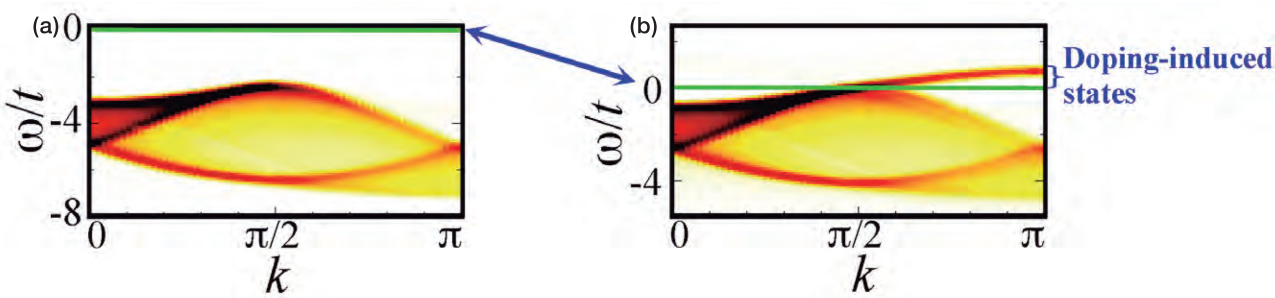

Fig. 1 Lower band of the electron excitation in the one-dimensional Hubbard model, taken from Ref. 1. **(a)** Mott insulator. **(b)** Doped Mott insulator. When the chemical potential (green line) touches the top of the lower band, a dispersing mode emerges just above the chemical potential.

Main Papers

1) "Spectral properties near the Mott transition in the one-dimensional Hubbard model", M. Kohno, *Phys. Rev. Lett.* **105** (2010) 106402.
2) "Mott transition in the two-dimensional Hubbard model", M. Kohno, *Phys. Rev. Lett.* **108** (2012) 076401.
3) "States induced in the single-particle spectrum by doping a Mott insulator", M. Kohno, *Phys. Rev. B* **92** (2015) 085129.

40 Making the invisible enemy visible: naked-eye cesium detection

W. Nakanishi, K. Ariga Co-workers: T. Mori, H. Komatsu, M. Akamatsu

Micrometer-level naked-eye detection of cesium (Cs) ions, a major source of contamination upon nuclear plant explosion, has been demonstrated. In this research, a substituted phenol compound containing an electron-accepting 4-nitrophenyl ether group was designed. The compound exhibited distinctive green fluorescence in the presence of Cs ions even in soil samples. This probe molecule is now commercialized and being applied for Cs ion detection in living cells.

Various sensing molecules for the detection of toxic or useful substances in the environment have been explored. Specifically, micrometer-level naked-eye detection of Cs ions, a major source of contamination after nuclear power plant explosions, has been demonstrated.

As a result of the accident at the Fukushima No. 1 Nuclear Power Plant following the Great East Japan Earthquake in March 2011, large amounts of radioactive substances leaked and contaminated a wide area. Among those substances, Cs-137 will continue to be a source of radiation in the future. The Japanese government has planned and implemented decontamination measures for the region contaminated by radioactive substances. However, if the distribution of Cs can be visualized, this decontamination work can be carried out more efficiently, and a reduction in the amount of contaminated waste generated by the decontamination can also be expected.

We developed a fluorescent probe that detects Cs using supermolecular interaction (Fig. 1(a)). This optical probe emits green fluorescent light when it contains Cs, thereby enabling visual confirmation of Cs distributed on the surface of a solid (Fig. 1(b)). It has higher spatial resolution than previous methods for detecting radioactive substances, allowing visualization of Cs distribution with sub-millimeter accuracy. Because this enables the selective removal of only Cs-contaminated spots, a major reduction in the amount of contaminated waste generated by decontamination work can be expected.

The probe is sensitive to Cs concentrations of 1 part per million (Cs^+/K^+). When an alcoholic solution of the optical probe is sprayed on plant leaves grown in the presence of Cs, the distribution of Cs ions within living cells can be visualized under flourescence microscopy (Fig. 1(c)). Because the probe molecule is now commercialized, it can be widely used for environmental remediation.

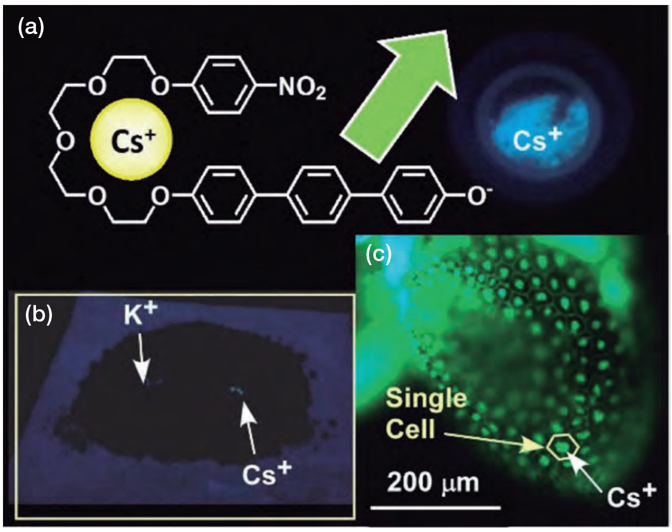

Fig. 1(a) Cs detection probe molecule and detection based on fluorescence emission on **(b)** the ground and in **(c)** living plant cells.

Main Papers

1) "Micrometer-level naked-eye detection of caesium particulates in the solid state", T. Mori, M. Akamatsu, K. Okamoto, M. Sumita, Y. Tateyama, H. Sakai, J.P Hill, M. Abe, K. Ariga, *Sci. Technol. Adv. Mater.* **14** (2013) 015002.

2) "Intracellular imaging of cesium distribution in Arabidopsis using Cesium Green", M. Akamatsu, H. Komatsu, T. Mori, E. Adams, R. Shin, H. Sakai, M. Abe, J.P. Hill, K. Ariga, *ACS Appl. Mater. Interfaces* **6** (2014) 8208.

41 Solid-state lithium-ion batteries: nanoarchitecture at the cathode interfacial

K. Takada, T. Ohnishi, M. Osada, T. Sasaki

Solid-state batteries are anticipated to be a fundamental solution to issues in lithium-ion batteries originating from their liquid electrolytes. Because they have low power density, a challenge is achieving practical power by enhancing ionic conduction in batteries made of solids. Nanomaterials have not found their place in batteries, since they are too small to store energy electrochemically. However, interfaces are often highly resistive and thus rate determining in solid-state systems, where nanomaterials will find their niche.

Although low ionic conductivities of solid electrolytes have been the reason for the low power of solid-state batteries, the highest conductivities found recently have exceeded 10^{-2} S/cm among sulfides, which have had ion transport in bulk cease from rate determination. However, even such sulfides have a drawback in ion transport: they show high resistance at the interface with high-voltage cathodes. Our previous studies revealed that surface coating of cathode materials with oxide-based solid electrolytes successfully reduces the interfacial resistance to achieve practical power density in solid-state batteries[1). The coating layer should be as thin as possible so as not to be resistive. One material for the interposition is the TaO_3^- nanosheet.

The TaO_3^- nanosheet is 1 nm thick and resembles a mesh in the crystal structure. Some of its openings are almost the same size as lithium ions to act as conduction channels for lithium ions, as illustrated in Fig. 1(a), and its band gap is as wide as 5.3 eV to make the nanosheet electronically insulating. Consequently, TaO_3^- nanosheets coated on the cathode surface reduce the interfacial resistance as the world's thinnest oxide electrolyte layer[2).

Thin-film oxide electrolytes sometimes form on the cathode material surface spontaneously. When Al is introduced to $LiCoO_2$, which is a typical cathode material, most Al substitutes for Co to form solid solutions of $LiAl_xCo_{1-x}O_2$, while the rest aggregates at the surface to form Al-enriched layers. Although $LiCoO_2$ is a mixed conductor, enriched Al suppresses the electronic conduction to change the surface to an ionic conductor. As a result, an oxide electrolyte layer is formed spontaneously in Al-substituted $LiCoO_2$, and high power density is achievable without any intentional coating[3).

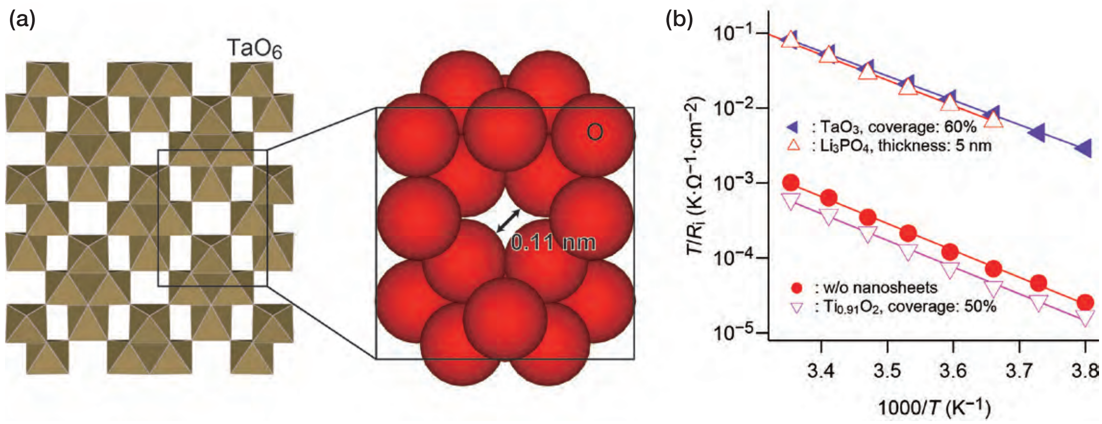

Fig. 1(a) Crystal structure of the TaO_3^- nanosheet and **(b)** its effects on interfacial resistance. The polyhedral representation illustrates its mesh structure, and the openings are almost the same size as lithium ions, which can be seen in the space-filling representation. The nanosheet reduces the interfacial resistance (R_i) by two orders of magnitude, as the oxide solid electrolyte Li_3PO_4 does, while a different nanosheet without openings, $Ti_{0.91}O_2$, does not.

Main Papers

1) "Enhancement of the high-rate capability of solid-state lithium batteries by nanoscale interfacial modification," N. Ohta, K. Takada, L. Q. Zhang, R. Z. Ma, M. Osada, T. Sasaki, *Adv. Mater.* **18** (2006) 2226.

2) "Tantalum oxide nanosheet as self-standing one nanometer thick electrolyte", X. X. Xu, K. Takada, K. Fukuda, T. Ohnishi, K. Akatsuka, M. Osada, B.T. Hang, K. Kumagai, T. Sekiguchi, T. Sasaki, *Energy Environ. Sci.* **4** (2011) 3509.

3) "Self-organized core–shell structure for high-power electrode in solid-state lithium batteries," X. X. Xu, K. Takada, K. Watanabe, I. Sakaguchi, K. Akatsuka, B. T. Hang, T. Ohnishi, T. Sasaki, *Chem. Mater.* **23** (2011) 3798.

42 Silicene: novel two-dimensional material with spin–orbit interaction

R. Arafune

With the great success of graphene, a novel two-dimensional honeycomb lattice was explored. Silicene, a honeycomb lattice of silicon atoms, has emerged as a rising star. We succeeded in synthesizing silicene on Ag (111). Using several state-of-the-art techniques to characterize the solid surfaces, we revealed the geometric and electronic structure of the silicene on Ag (111).

Silicene, a 2D honeycomb lattice sheet consisting of Si atoms, has attracted much attention as a novel quantum physics testing field because it gains various fascinating characteristics due to combination of the Dirac fermion with spin-orbit interaction. Unlike graphene, silicene does not have a "mother material" such as graphite and thus should be grown on solids. We found that silicene can be grown on Ag(111), as shown in Fig. 1(a). The geometric arrangement of silicene on Ag(111) was determined using scanning tunneling microcopy (STM), low-energy electron diffraction, and density functional theory (DFT) calculations. A prominent difference in the geometric arrangement of silicene compared with graphene is that on Ag(111) it takes a locally buckled structure in which Si atoms are displaced perpendicular to the basal plane, allowing superstructures such as 4×4, $\sqrt{13}\times\sqrt{13}$ R13.9°, $4/\sqrt{3}\times4/\sqrt{3}$, etc. to emerge.

The flexibility of silicene also affects the electronic structure. Buckling leads to nonnegligible coupling at the silicone-substrate interface. DFT calculations (Fig. 1(b)) show that the π and π^* bands derived from Si $3p_z$ are hybridized with the Ag electronic states, leading to drastic modification of the band structure and then absence of Dirac fermion features. No Landau-level sequences were observed by scanning tunneling spectroscopy with magnetic fields, and the parabolic dispersion curve is measured in the $4/\sqrt{3}\times4/\sqrt{3}$ phase (Fig. 1(c)). These findings demonstrate that strong coupling at the interface causes silicene symmetry breaking.

To summarize, we synthesized silicene, which does not exist in nature, and revealed its geometric and electronic properties. Silicene is more flexible than graphene, which enables tuning of the electronic structure through the substrate electronic system.

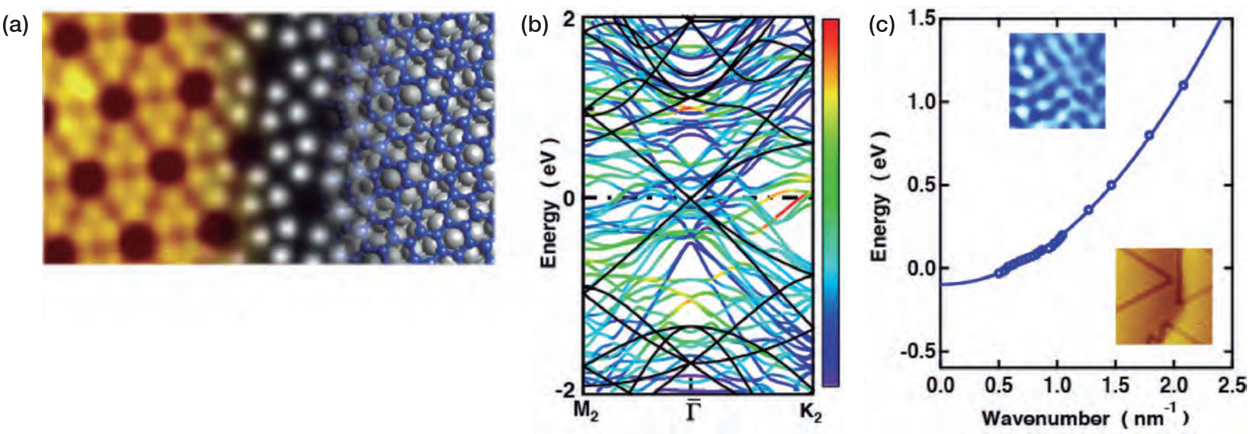

Fig. 1 Silicene on Ag(111). **(a)** STM image, DFT simulation, and ball model of silicene/Ag(111). **(b)** Calculated band structure. The black curves are for the freestanding and the colored are for 4x4 silicene/Ag(111). **(c)** Band dispersion of "multilayer silicene." Insets show the STM image and quasiparticle interference pattern.

Main Papers

1) "Structural transition of silicene on Ag(111)", R. Arafune, C.-L. Lin, K. Kawahara, N. Tsukahara, E. Minamitani, Y. Kim, N. Takagi, M. Kawai, *Surf. Sci.* **608** (2013) 297.
2) "Substrate-induced symmetry breaking in silicene", C.-L. Lin, R. Arafune, K. Kawahara, M. Kanno, N. Tsukahara, E. Minamitani, Y. Kim, M. Kawai, N. Takagi, *Phys. Rev. Lett.* **110** (2013) 076801/1-5.
3) "Silicene on Ag(111): geometric and electronic structures of a new honeycomb material of Si", N. Takagi, C.-L. Lin, K. Kawahara, E. Minamitani, N. Tsukahara, M. Kawai, R. Arafune, *Prog. Surf. Sci.* **90** (2015) 1.

World Premier International
Research Center Initiative

International Center for
Materials Nanoarchitetonics

National Institute for
Materials Science

International Center for
Materials Nanoarchitectonics (MANA)

1-1 Namiki, Tsukuba, Ibaraki, 305-0044 JAPAN
Phone +81-29-860-4709
Fax +81-29-860-4706
E-mail mana@nims.go.jp

http://www.nims.go.jp/mana/